

M³TR: Temporal Retrieval Enhanced Multi-Modal Micro-video Popularity Prediction

Jiacheng Lu*
Weijian Wang*
jack111@sjtu.edu.cn
SekaiWwj@sjtu.edu.cn
Shanghai Jiao Tong University
Shanghai, Shanghai, China

Xiaoming Yuan
Shanghai Jiao Tong University
Shanghai, Shanghai, China
xiaomy_mark@sjtu.edu.cn

Yang Hua
Queen’s University Belfast
Belfast, Northern Ireland, UK
Y.Hua@qub.ac.uk

Tao Song†
Shanghai Jiao Tong University
Shanghai, Shanghai, China
songt333@sjtu.edu.cn

Jiaru Zhang
Purdue University
West Lafayette, Indiana, USA
jiaru@purdue.edu

Bo Peng
Shanghai Jiao Tong University
Shanghai, Shanghai, China
pengbo_michael@sjtu.edu.cn

Cheng Hua
Shanghai Jiao Tong University
Shanghai, Shanghai, China
cheng.hua@sjtu.edu.cn

Haibing Guan
Shanghai Jiao Tong University
Shanghai, Shanghai, China
hbguan@sjtu.edu.cn

Abstract

Accurately predicting the popularity of micro-videos is a critical but challenging task, characterized by volatile, ‘rollercoaster-like’ engagement dynamics. Existing methods often fail to capture these complex temporal patterns, leading to inaccurate long-term forecasts. This failure stems from two fundamental limitations: ① a superficial understanding of user feedback dynamics, which overlooks the mutually exciting and decaying nature of interactions such as likes, comments, and shares; and ② retrieval mechanisms that rely solely on static content similarity, ignoring the crucial patterns of how a video’s popularity evolves over time. To address these limitations, we propose M³TR, a Temporal Retrieval enhanced Multi-Modal framework that uniquely synergizes fine-grained temporal modeling with a novel temporal-aware retrieval process for Micro-video popularity prediction. At its core, M³TR introduces a Mamba-Hawkes Process (MHP) module to explicitly model user feedback as a sequence of self-exciting events, capturing the intricate, long-range dependencies within user interactions (for **limitation** ①). This rich temporal representation then powers a temporal-aware retrieval engine that identifies historically relevant videos based on a combined similarity of both their multi-modal content (visual, audio, text) and their popularity trajectories (for **limitation** ②). By augmenting the target video’s features with this retrieved knowledge, M³TR achieves a comprehensive understanding of prediction. Extensive experiments on two real-world datasets demonstrate the superiority of our framework. M³TR achieves state-of-the-art performance, outperforming previous methods by up to 19.3% in nMSE and showing significant gains in addressing long-term prediction challenges.

1 Introduction

Micro Video Popularity Prediction (MVPP) has become a critical area of research and application with the rapid rise of short-form video platforms such as TikTok, YouTube Shorts and Instagram Reels [21]. MVPP aims to forecast the popularity of micro-videos based on content, context and user interactions. It is essential for enhancing recommendation systems [19, 35], enabling public sentiment analysis and control [43], optimizing targeted advertising [27], and guiding content creation strategies. MVPP offers multifaceted advantages, from empowering users to navigate the vast digital landscape more effectively to enhance applications like personalized marketing, social trend analysis, and content moderation [21]. In the context of this work, MVPP is defined not only as forecasting a single, static score, but as predicting the *temporal evolution* of a video’s user engagement metrics: likes, shares, and comments.

Previous research in MVPP can be broadly categorized into three main approaches: feature-based modeling, historical sequence modeling, and similarity-based modeling. Early feature-based methods focus on manually extracting static cues (e.g., image brightness and audio volume) but struggle with scalability and the complexity of modern content. More recent deep learning approaches have advanced behavior modeling by integrating user engagement metrics (e.g., likes and shares) with multi-modal features. However, these methods often treat user feedback as a simple aggregated time series, which leads to the **limitation** ①. They largely overlook the fine-grained, mutually exciting nature of user interactions, where a burst of likes might trigger a subsequent wave of shares, or negative comments might inhibit future growth.

To overcome the problems of learning from a single video’s data, retrieval-based methods have gained attention. These approaches enhance predictions by leveraging a vast repository of historical videos, retrieving similar content to inform the forecast [6, 45]. While promising, the effectiveness of these methods is often capped

*Both authors contributed equally to this research.

†Corresponding author

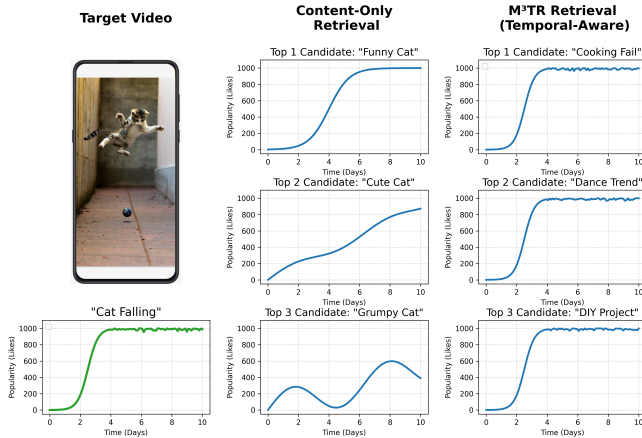


Figure 1: Illustration of the core motivation for M^3TR . Given a target video (left) exhibiting a “flash-in-the-pan” popularity trajectory, a conventional Content-Only Retrieval system (middle) identifies videos that are thematically similar (e.g., other cat videos) but whose popularity patterns are fundamentally different, offering poor predictive value. In stark contrast, our M^3TR Retrieval (right), which is temporal-aware, retrieves videos with entirely different content (e.g., “cooking fail” and “dance trend”) but nearly identical popularity trajectories. This demonstrates that the temporal user feedback of videos is a critical predictive signal that is missed by content-centric approaches.

by a reliance on static, content-centric similarity. As shown in Figure 1, a typical retrieval system might correctly match a target video of a cat with other cat videos. However, it fails to recognize that their differing popularity dynamics offer poor, or even misleading, predictive signals. The system completely misses thematically different videos (e.g., a “dance trend” or “DIY project”) that share an identical viral pattern—a crucial piece of information for an accurate forecast. The **limitation** ② stems from their inability to measure and retrieve based on temporal similarity, leaving a significant source of predictive power untapped (Appendix [A](#)).

To address these two fundamental limitations mentioned above, we propose M^3TR , a novel Temporal Retrieval enhanced Multi-Modal framework for Micro-video popularity prediction. M^3TR introduces a paradigm shift by positing that accurate prediction requires synergizing deep temporal dynamic modeling with a temporal-aware retrieval process. Our contributions are threefold:

(i) We propose a novel framework, M^3TR , that for the first time, integrates a sophisticated temporal event model directly into a multi-modal retrieval pipeline, bridging the gap between user behavior modeling and retrieval augmentation. (ii) We introduce a (1) **Mamba-Hawkes Process (MHP) module** to explicitly capture the long-range, self-exciting, and mutually-influential dynamics within user feedback sequences, providing a far richer temporal representation than previous methods. This representation is then leveraged by our (2) **temporal-aware retrieval engine**, which computes similarity based on both multi-modal content and the temporal patterns captured by the MHP. This integrated approach

uniquely enables the discovery of videos that share similar popularity trajectories, regardless of their underlying content. (iii) We conduct extensive experiments on two large-scale, real-world datasets, demonstrating that M^3TR significantly outperforms state-of-the-art methods by up to **19.3%**.

2 Related Work

Current research primarily focuses on three approaches: feature-based modeling, historical sequence modeling, and similarity-based modeling.

Feature-based modeling derives predictive signals from video static and dynamic attributes (titles, thumbnails, comments, etc.) [2]. Evolutions range from early CNN/RNN models processing low-level cues (e.g., brightness) paired with XGBoost [33], to Bi-LSTM extracting higher-order semantics [17], and recent attention-based multi-modal fusion capturing contextual patterns [18, 31, 40]. For instance, the AMPS [8] integrates features across multiple time windows, effectively combining global and local data to improve prediction accuracy. Despite model advances, two fundamental flaws persist: aggregated features fail to capture temporal dynamics, and semantic-rich features (emotion/object interactions) suffer from poor cross-context generalizability.

Historical sequence modeling leverages the analysis of past viewing data and user behavior to capture temporal trends in video popularity. Traditional time series methods, such as ARIMA [36], are commonly employed for short-term forecasting but struggle with complex nonlinear patterns. To address this, researchers have proposed contextual popularity modeling approaches that extract inherent patterns from viewing data to predict future trends [1]. Additionally, social network-based approaches utilize graph analysis to model the dynamic dissemination of videos within networks, forecasting their future popularity trajectories [41]. However, these methods only focus on social network analysis and lack the integration with intrinsic video content features which in fact limits their applicability.

Retrieval-based modeling improves popularity prediction accuracy by analyzing video relationships, which have also gained prominence in recent years. For example, the MMRA method combines visual and textual information to retrieve similar videos from the memory network [45]. RAGTrans [6] employs a multi-modal memory database and hypergraph-based enhancements to generate robust representations of user-generated content, thereby improving social media popularity forecasts. These methods inherently offer interpretability by grouping similar content clusters, but they fail to exploit temporal patterns of videos with similar user feedback.

3 Methodology

3.1 M^3TR Framework Overview

Let $\mathcal{V} = \{V_1, V_2, \dots, V_N\}$ be a collection of micro-videos. Each video V_i is a composite of multi-modal data streams, including visual frames, audio tracks, and textual metadata (e.g., titles and descriptions). Accompanying each video is a time-stamped sequence of user interactions, such as likes, shares, and comments. The goal of Micro-Video Popularity Prediction (MVPP) is to learn a function $\psi(\cdot)$ that takes the multi-modal content and user interaction history

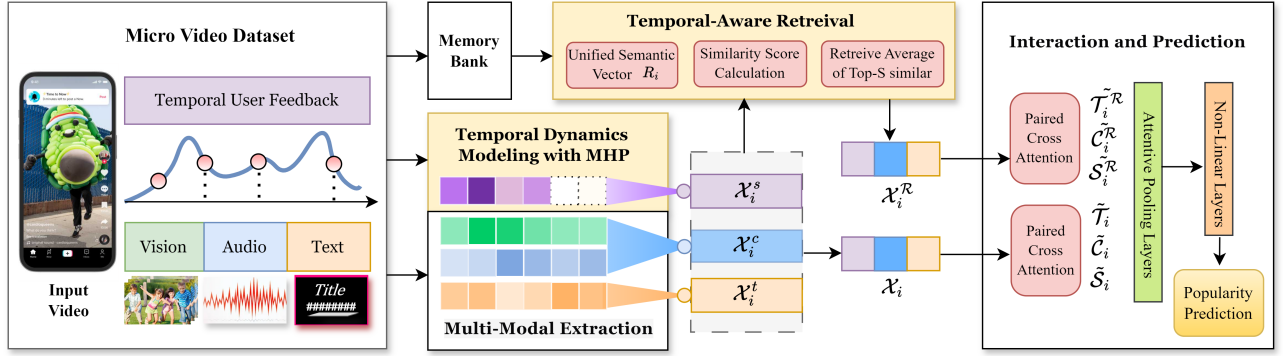


Figure 2: Overall framework. The workflow begins with two input streams: the Input Video, from which multi-modal features (vision, audio, text) are extracted, and its corresponding temporal user feedback. M^3TR employs a Multi-Modal Extraction module for vision, audio and text. Meanwhile, it applies Temporal Dynamics Modeling with a Mamba-Hawkes Process (MHP) for temporal user feedback, which explicitly captures the long-range, self-exciting nature of user interactions, generating a sophisticated temporal feature representation (X_i^s). This rich temporal feature powers the other core innovation of our framework: the Temporal-Aware Retrieval engine. Unlike conventional methods that rely on static content similarity, our engine queries the Memory Bank to identify historical videos based on a combined similarity of both their popularity trajectories (derived from X_i^s) and their multi-modal content. It retrieves and averages the features of the most relevant historical examples to form an augmented feature vector (X_i^R). Finally, in the Interaction and Prediction stage, the model fuses the video’s original multi-modal features (X_i) with the retrieved temporal-aware features (X_i^R) using Paired Cross Attention. The resulting representation is then refined through Attentive Pooling and Non-Linear Layers to generate the final Popularity Prediction.

of a video V_i as input and predicts a vector of its future popularity metrics, $\hat{Y}_i = [\hat{y}_{likes}, \hat{y}_{shares}, \dots]$.

To tackle this challenge, we propose the M^3TR framework, whose overall architecture is illustrated in Figure 2. M^3TR firstly extracts features of multi-modalities, and specifically models temporal dynamics for user feedback. Then the data flows into a temporal-aware retrieval module to enhance feature exploitation. The final step is to integrate the retrieved information with the target video’s features to make a dynamic prediction.

3.2 Temporal Dynamics Modeling with MHP

As mentioned in Sec 2, a core limitation of prior work is its failure to capture the rich dynamics of user engagement. However, user interactions are not independent; for example, they form a cascade of influence where likes can inspire comments, and shares can trigger new views. To model these user interactions, we treat the users’ feedback sequence as a *multivariate self-exciting point process*. We thereby propose the **Mamba-Hawkes Process (MHP)**, a novel architecture that captures these intricate temporal dependencies to generate a history-aware representation of a video’s popularity trajectory.

3.2.1 The Mamba-Hawkes Process Model. Let a user’s response sequence be $\mathcal{R} = \{(t_0, \gamma_0), (t_1, \gamma_1), \dots, (t_n, \gamma_n)\}$, where t_i is the time-tamp and γ_i is a one-hot vector indicating the event type (e.g., like and share). The core of our MHP model is its intensity function $\lambda_k(t)$, which defines the instantaneous probability of an event of type k occurring at time t . We formulate this intensity to include a

classical self-exciting component augmented by a dynamic, non-linear context learned by a Mamba network (refer to Appendix B and Appendix C for explanation):

$$\lambda_k(t) = \text{softplus}\left(\mu_k + \sum_{m=1}^M \sum_{t_j^{(m)} < t} \alpha_{k,m} e^{-\delta_{k,m}(t-t_j^{(m)})}\right) + f_k(\mathbf{h}(t)), \quad (1)$$

where μ_k is the baseline intensity for event type k ; The summation term models the linear, exponentially decaying influence of past events $t_j^{(m)}$ of type m on the current intensity of type k , governed by excitation coefficients $\alpha_{k,m}$ and decay rates $\delta_{k,m}$; $f_k(\mathbf{h}(t))$ is a non-linear function whose input, $\mathbf{h}(t)$, is a history-aware hidden state produced by a Mamba network. Moreover, to strictly enforce the non-negativity constraint required by point process definitions, we apply a link function, $\lambda_k(t) = \text{softplus}(\cdot)$, to the entire intensity function. It is worth noting that the term $f_k(\mathbf{h}(t))$ allows the model to capture complex, long-range dependencies that the classical component cannot (refer to Appendix C.9).

Dynamic Context with Mamba. The Mamba architecture [15] is uniquely suited to compute the dynamic context $\mathbf{h}(t)$ due to its efficiency in modeling long sequences. As illustrated in Figure 3, it processes the sequence of embedded event vectors, $v_{t_i} = \gamma_i E^T$, where $E \in \mathbb{R}^{d \times M}$ is a learnable embedding matrix. Mamba maintains a compressed hidden state ζ_{t_i} , which is updated at each event time t_i based on the time difference $\Delta t_i = t_i - t_{i-1}$ and the current

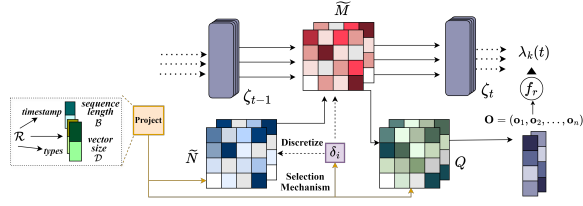


Figure 3: The Mamba-Hawkes Process (MHP) Architecture. It computes a dynamic intensity function by combining a classical Hawkes process with a non-linear context vector generated by a Mamba network that processes the entire event history.

event embedding v_{t_i} . This update mechanism, based on a structured state-space model (SSM), allows it to selectively recall or forget information over long horizons, yielding a rich final hidden representation $\mathbf{h}(t)$ that informs the intensity function (refer to Appendix [M](#) for a demo case of MHP’s function).

3.2.2 Sequence Generation via NHPP Simulation. Deep learning models typically require fixed-length inputs, but user interaction sequences are variably-lengthed. To address this, we treat the event sequence as a Non-Homogeneous Poisson Process (NHPP) governed by our learned intensity $\lambda_k(t)$ from Eq. (1). We then employ **Ogata’s thinning algorithm** [5] to simulate events from this process, augmenting shorter sequences to a desired fixed length in a statistically principled manner (refer to Appendix [D](#)).

The thinning algorithm first establishes a constant upper bound $\lambda_{\max}^{(k)}$ for the intensity function over the simulation interval. It then generates candidate events from a simpler, computationally efficient homogeneous Poisson process with rate $\lambda_{\max}^{(k)}$. Finally, each candidate event at time t_{cand} is stochastically “thinned” (i.e., accepted or rejected) with an acceptance probability of $\lambda_k(t_{\text{cand}})/\lambda_{\max}^{(k)}$. This procedure generates a padded event sequence whose statistical properties are faithful to our complex MHP intensity function. The final output of this module is a fixed-length temporal embedding, X_i^t , derived from this complete event sequence, which serves as the temporal signature of video V_i for our downstream retrieval task.

3.2.3 Theory Analysis. To ensure the statistical soundness of our temporal modeling, we formally state and prove that the estimator for the parameters of the Mamba-Hawkes Process (MHP) possesses desirable oracle properties [28]. This is crucial as the MHP module forms the core of our temporal feature extraction pipeline. The “oracle property” implies that, with enough data, our parameter estimator behaves as if it knew in advance.

THEOREM 3.1 (ORACLE PROPERTIES OF THE MHP ESTIMATOR). *Let the d -dimensional counting process $N(t)$ be generated by a multivariate Hawkes process with its true conditional intensity vector governed by a sparse parameter vector $\theta^* \in \mathbb{R}^p$. Let $A = \{j | \theta_j^* \neq 0\}$ be the true active set of size $|A| = q \ll p$. The estimator $\hat{\theta}_N$ is obtained by maximizing the penalized log-likelihood from N i.i.d. observed video*

interaction sequences over a time horizon T :

$$\hat{\theta}_N = \arg \max_{\theta \in \mathbb{R}^p} \left\{ L_N(\theta) - \sum_{j=1}^p p_{YN}(|\theta_j|) \right\}, \quad (2)$$

where $L_N(\theta)$ is the normalized log-likelihood, and $p_{YN}(\cdot)$ is a non-concave penalty function such as MCP [42], with regularization parameter γ_N .

Under standard regularity assumptions (formally stated in Appendix G), the estimator $\hat{\theta}_N$ possesses the oracle property. That is, as $N \rightarrow \infty$:

- (1) **Sparsity Recovery:** The estimator correctly identifies the true zero and non-zero parameters with probability approaching one. Formally, $P(\{\hat{\theta}_{N,j} \neq 0\} = A) \rightarrow 1$.
- (2) **Asymptotic Normality:** The estimator for the non-zero parameters, $\hat{\theta}_{N,A}$, is asymptotically normal and has the same asymptotic distribution as the oracle estimator, which knows the true active set A beforehand.

$$\sqrt{N}(\hat{\theta}_{N,A} - \theta_A^*) \xrightarrow{d} \mathcal{N}(0, I_{A,A}(\theta^*)^{-1}),$$

where $I_{A,A}(\theta^*)$ is the Fisher information matrix for the non-zero parameters, evaluated at the true parameter θ^* .

The proof is provided in Appendix [G](#).

3.3 Temporal-Aware Retrieval

Having established a method to generate powerful temporal embeddings in Section 3.2, we now describe how to leverage this information for prediction. A video’s popularity is often correlated with that of existing, similar videos. However, “similarity” is twofold: videos can be similar in their *content* (e.g., visual themes, topics) or in their *popularity dynamics* (e.g., a slow burn vs. a viral explosion). Our framework’s core hypothesis is that the most relevant videos for retrieval are those that are similar on **both** axes. To this end, we design a temporal-aware retrieval module.

For each video V_i in our dataset, we first extract a set of feature embeddings and are stored in a memory bank, representing its multi-modal content and its temporal signature. Aligning all modalities, we generate unified semantic vectors, calculate the similarity scores and retrieves the top- S most similar videos from a pre-built memory bank.

Multi-modal Content Embeddings (X_i^c, X_i^t). We employ standard, pre-trained models to encode the primary content modalities. Visual features from keyframes are processed by a Vision Transformer (ViT) [9], while corresponding audio segments are processed by an Audio Spectrogram Transformer (AST) [13]. The resulting embeddings are concatenated and passed through a linear layer to produce a unified audio-visual embedding, $X_i^c \in \mathbb{R}^{K \times d}$. Textual metadata is encoded using the AngLE sentence embedding model [30] to produce a text embedding, $X_i^t \in \mathbb{R}^{n_w \times d}$. Further implementation details are deferred to Appendix [E](#).

Temporal Dynamics Embedding (X_i^s). The temporal signature of the video, X_i^s , is the fixed-length event sequence embedding generated by our Mamba-Hawkes Process module, as detailed in Section 3.2. This vector is a rich summary of the video’s engagement trajectory.

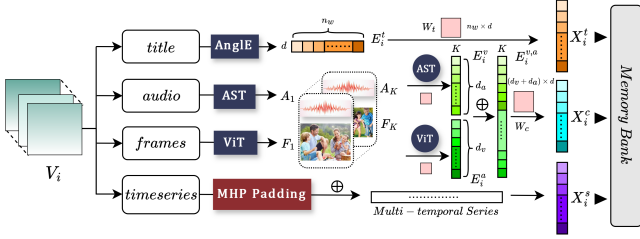


Figure 4: Multi-modal/temporal Feature Extraction for Memory Bank Prebuild. Visual, acoustic, textual and time-serial features of videos are extracted and encoded into embeddings through various mechanisms. These processed embeddings are also restored for subsequent retrieval.

Unified Semantic Vector (R_i). To facilitate a robust content-based similarity search, we unify the different modalities into a common textual semantic space. We use pre-trained vision-to-text BLIP-2 [29] and audio-to-text CLAP [38] models to generate descriptive captions for the video’s visual and audio content, respectively. These generated captions are concatenated with the original textual description and encoded using AngLE to produce a single, holistic semantic retrieval vector R_i . This vector serves as the primary key for content-based similarity.

Similarity Score Calculation. With these representations, we compute a unified similarity score $SS(V_i, V_j)$ between a target video V_i and a candidate video V_j from the memory bank. This score is a composition of two distinct similarity measures. $SS_{\text{modal}}(V_i, V_j) = R_i \cdot R_j^T$ represents the content-level similarity using the unified semantic vectors, and $SS_{\text{temp}}(V_i, V_j) = \text{mean_pool}(X_i^s) \cdot \text{mean_pool}(X_j^s)^T$ measures the similarity in popularity dynamics using the MHP-derived temporal embeddings.

To balance the influence of both modalities and ensure their scales are comparable, we first apply Min-Max normalization to map each similarity score to the range $[0, 1]$. We then combine them using the L2-norm to produce the final temporal-aware similarity score:

$$SS(V_i, V_j) = \sqrt{\text{Norm}(SS_{\text{modal}})^2 + \text{Norm}(SS_{\text{temp}})^2}. \quad (3)$$

Memory Bank Retrieval. Our memory bank \mathcal{B} stores the complete set of feature embeddings for all videos in the training corpus:

$$\mathcal{B} = \{(X_1^c, X_1^t, X_1^s, R_1, Y_1), \dots, (X_N^c, X_N^t, X_N^s, R_N, Y_N)\}. \quad (4)$$

For a given target video V_i , we compute its similarity $SS(V_i, V_j)$ with every video $V_j \in \mathcal{B}$. We then identify the set \mathcal{V}_i^R containing the top- S videos with the highest similarity scores. The feature embeddings and ground-truth popularity labels of this retrieved set $\{(X_j^c, X_j^t, X_j^s, Y_j)\}_{V_j \in \mathcal{V}_i^R}$ are then passed to our final integration module (Section 3.4) to serve as augmented knowledge for the prediction task. The overall retrieval process is depicted in Figure 5.

3.4 Interaction and Prediction

Once the top- S similar videos are retrieved from the memory bank, the final step is to fuse this augmented information with the target

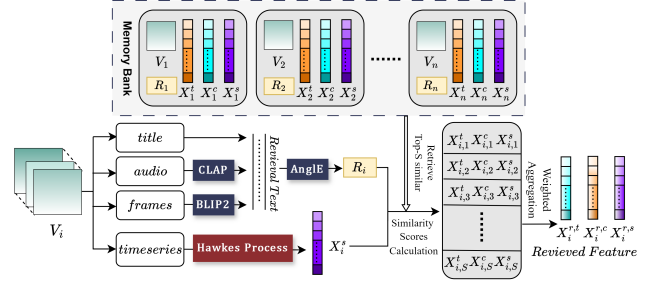


Figure 5: Temporal-Aware Retrieval. Similarity scores could be computed by aligning visual, acoustic and textual features and incorporating time-serial embeddings. Analogous videos with the highest similarity scores are then retrieved from memory bank for follow-up integration process.

video’s features to make a prediction. This process involves two levels of interaction: aligning features within each video (intra-video) and then integrating information across the target and retrieved videos (inter-video).

Intra-Video Modal Alignment. To create a holistic representation for the target video V_i , we must first resolve potential inconsistencies between its audio-visual (X_i^c), textual (X_i^t), and temporal (X_i^s) embeddings. We employ a series of cross-attention networks to achieve this alignment. For instance, to enrich the textual features with visual context, we query the visual embeddings with the textual embeddings, and vice versa. This process yields a set of enhanced, modality-aligned representations $(\tilde{C}_i, \tilde{T}_i, \tilde{S}_i)$, where each vector is now infused with context from the other modalities. The same alignment process is applied independently to each of the S retrieved videos. The detailed mechanism is provided in Appendix [F.1](#).

Retrieval-Enhanced Fusion and Prediction. The core of our retrieval augmentation lies in effectively integrating the knowledge from the retrieved set, \mathcal{V}_i^R . We achieve this by constructing a *cross-sample interaction vector* \mathcal{I}_i , which captures the relationships between the target video and its retrieved neighbors. This vector is formed by computing the inner product between the aligned representations of the target video and those of the retrieved videos.

Finally, all available information is concatenated into a single feature vector H_i :

$$H_i = \text{concat} \left([\tilde{C}_i, \tilde{T}_i, \tilde{S}_i] \oplus \{\tilde{C}_j^R, \tilde{T}_j^R, \tilde{S}_j^R, Y_j\}_{V_j \in \mathcal{V}_i^R} \oplus \mathcal{I}_i \right), \quad (5)$$

where we include the aligned features of the retrieved videos as well as their ground-truth popularity labels Y_j as explicit guidance. This comprehensive vector H_i is fed into a non-linear layer to predict the popularity score \hat{Y}_i for the target video. Detailed architecture is shown in Appendix [F.2](#).

Training Pipeline and Data Leakage Prevention. Our model is trained end-to-end. We use a combined loss $L = L_{\text{pred}} + \gamma L_{\text{mhp}}$, where L_{pred} is the nMSE regression loss for the final popularity prediction, and L_{mhp} is the negative log-likelihood of the MHP module (as described in Sec. 3.2.3). To strictly prevent data leakage: (1) During training, when retrieving neighbors for a target video

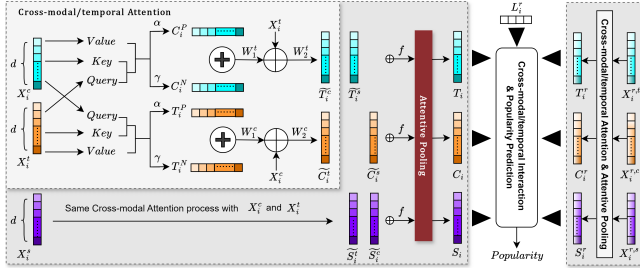


Figure 6: Cross-modal/temporal Attention and Interaction with Retrieval Enhancement. Feature embeddings of both the target video and retrieved videos are integrated through cross-modal attention and interaction, which finally generate the comprehensive popularity prediction.

V_i , V_i itself is explicitly excluded from the retrieval candidate pool. (2) At test time, the retrieval module queries only the memory bank built from the training set. No features or labels from the test set are present in the memory bank during inference. Thus, the ground-truth labels Y_j used in Eq. 5 are always from training samples.

4 Experiments

4.1 Datasets

To evaluate the effectiveness of M^3TR , we conduct experiments on the micro-video dataset: **MicroLens-100k** [32]. Another dataset we employ is the Tiktok Micro-video training-set which is provided by the **2024 INFORMS Data Challenge** committee. While the public INFORMS 2024 dataset only provides a single timestamp per video, our participation in the challenge granted us access to the full event-level user interaction sequences (e.g., likes, comments, shares with timestamps), which are used in this study for our Mamba-Hawkes Process module. The detailed information of these two datasets and other existing datasets that we thoroughly reviewed are in Appendix [J](#).

4.2 Implementation

4.2.1 Evaluation Metrics. We adopt the normalized Mean Square Error (nMSE) as the main parameter to measure the performance, and report Spearman’s Rank Correlation (SRC) coefficient, Pearson linear correlation coefficient (PLCC), and Mean Absolute Error (MAE). Detailed metric definition is displayed in Appendix [K](#).

4.2.2 Experimental Settings. All our experiments are conducted on a Linux server with 4 RTX 3090 GPUs. More detailed experimental settings are provided in Appendix [L](#).

4.2.3 Hyper-Parameter Settings. We adopt the Bayesian Optimization [24], searching through the parameter hyper-space, and find the lowest nMSE when setting [learning_rate, batch_size, weight_decay, dropout, α , K]=[1e-5, 64, 0.001, 0, 0.8, 10]. We apply the above set of parameters to acquire our result and compare M^3TR with other baselines.

4.3 Performance Comparison

4.3.1 Baseline Models. To evaluate our model, we conduct experiments with 9 competitive baselines of different methods, including SVR [25], HyFea [26], CLSTM [12], TMALL [3], MASSL [4], CBAN [7], HMMVED [39], MTFM [44] and MMRA [45]. Detailed information is summarized in Appendix [I](#).

4.3.2 Performance. The performance of baseline models and our model on the dataset is presented in Table 1. The results demonstrate that M^3TR outperforms all baselines.

4.4 Ablation Study

4.4.1 Qualitative Analysis. The importance of our Mamba-Hawkes Process (MHP) module is best illustrated through a qualitative case study. Figure 8 visualizes a complex scenario where an initial surge of positive interactions (Likes) is followed by a wave of controversial Comments. The classic Hawkes process (green dashed line), only observing the self-exciting nature of likes, erroneously predicts a continued, explosive growth. In contrast, our Mamba component learns the complex, cross-modal dependency and provides a crucial negative correction (red shaded area), recognizing that controversial comments suppress future like activity. The final MHP intensity (blue solid line) accurately models the resulting stall in engagement. This case study demonstrates the MHP’s unique ability to capture nuanced, non-linear dynamics that simpler temporal models miss. A more detailed breakdown of this case study is in Appendix [M.1](#). And we present a detailed qualitative case study across various popularity archetypes in Appendix [M.2](#) to further provide an intuitive understanding of these dynamics.

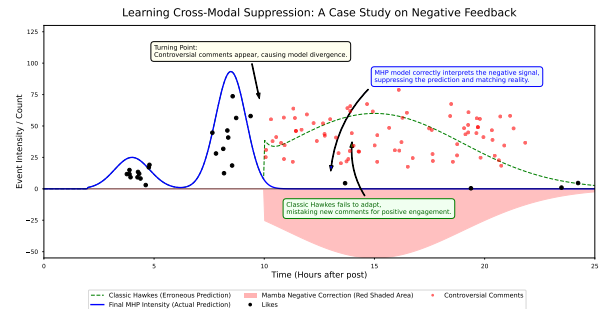


Figure 8: A case study visualizing the internal dynamics of the MHP module, demonstrating its ability to handle complex, cross-modal signals. This chart contrasts two predictive models tracking a video’s engagement. Initially, both the ‘Final MHP Intensity’ (blue solid line) and the ‘Classic Hawkes’ model (green dashed line) observe a series of ‘Likes’ (black dots). However, after the 10-hour mark, a new cross-modal event occurs: a wave of ‘Controversial Comments’ (red dots). The ‘Classic Hawkes’ process, which is blind to this new temporal signal, fails to adapt and erroneously predicts continued engagement growth. In sharp contrast, our Mamba component detects the suppressive nature of these comments and introduces a ‘Mamba Negative Correction’ (red shaded area). This crucial correction allows our ‘Final MHP Intensity’ (blue solid line) to accurately model the real-world outcome.

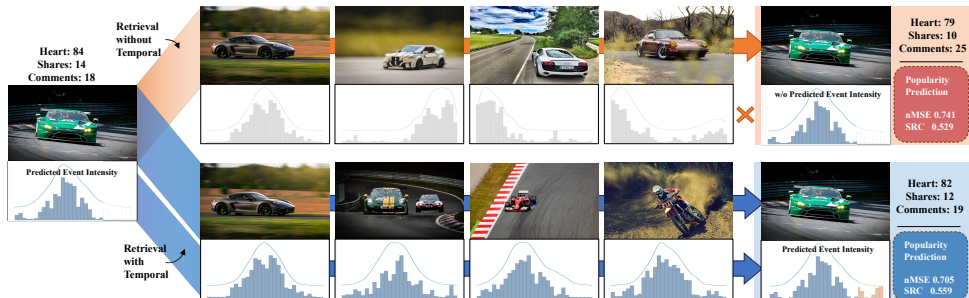


Figure 7: Qualitative experimental test results comparing traditional content-only retrieval with M^3TR temporal-aware retrieval. The target video (left) has a ground truth popularity, and its predicted event intensity follows a distinct bell curve. Top Row (Retrieval without Temporal): The conventional content-only method retrieves thematically similar videos (other cars). However, their popularity trajectories are flat and dissimilar, offering poor predictive signals. This reliance on irrelevant patterns leads to an inaccurate prediction and poor experimental test metrics. Bottom Row (Retrieval with Temporal): In contrast, our M^3TR framework retrieves videos that share a similar *temporal DNA*—a matching bell-shaped intensity curve—even if the content is not identical.

Model	MicroLens-100k				2024 INFORMS Data Challenge Dataset			
	nMSE(↓)	SRC(↑)	MAE(↓)	PLCC(↑)	nMSE(↓)	SRC(↑)	MAE(↓)	PLCC(↑)
CBAN	0.817±0.021	0.466±0.023	25.20±1.29	0.429±0.018	0.941±0.051	0.221±0.014	39.03±1.85	0.350±0.018
CLSTM	0.842±0.032	0.471±0.021	25.53±1.41	0.421±0.024	0.936±0.049	0.316±0.018	42.17±2.71	0.316±0.019
HMMVED	0.893±0.040	0.353±0.013	27.40±1.32	0.323±0.014	0.951±0.042	0.262±0.014	45.63±2.28	0.199±0.014
MASSL	0.927±0.046	0.380±0.026	25.16±1.26	0.329±0.014	1.004±0.059	0.251±0.017	40.90±2.25	0.251±0.014
SVR	1.019±0.051	0.405±0.015	25.04±1.40	0.321±0.013	1.203±0.066	0.285±0.018	45.45±2.77	0.229±0.013
MFTM	0.876±0.031	0.414±0.011	26.42±1.37	0.352±0.025	0.990±0.054	0.301±0.021	44.66±2.93	0.292±0.019
MMRA	0.785±0.024	0.495±0.025	24.34±1.21	0.480±0.020	0.911±0.050	0.387±0.026	39.21±2.26	0.373±0.025
Hyfea	0.840±0.039	0.432±0.022	26.10±1.38	0.408±0.022	0.953±0.058	0.245±0.019	36.81±2.84	0.284±0.016
TMALL	0.856±0.033	0.440±0.022	26.11±1.22	0.401±0.028	0.913±0.042	0.296±0.021	40.20±2.45	0.345±0.020
M^3TR	0.705±0.020	0.559±0.024	23.10±1.01	0.557±0.025	0.854±0.037	0.433±0.020	31.64±1.59	0.406±0.016

Table 1: Performance Comparison of Baselines and M^3TR

4.4.2 *Quantitative Results.* The quantitative results in Table 2 strongly corroborate these qualitative findings across three key dimensions: overall architecture robustness, temporal modeling strategies, and multi-modal integration.

First, analyzing the four primary variants (Table 2, Left), the substantial performance drop in the **noTemporal** and **noMHP** variants highlights that temporal dynamics are indispensable. Our full M^3TR model not only achieves the best overall metrics but also maintains the most accurate predicted popularity scores across stratified Top and Bottom groups, confirming its robustness for both highly popular (head) and less popular (tail) videos.

Second, evaluating different temporal modeling strategies (Table 2, Top Right) validates *how* these dynamics must be captured. Simple methods like Padding&Masking and the Poisson Process fail to effectively model temporal information. While the Neural Hawkes Process improves performance, our Mamba Hawkes Process (MHP) achieves the best results. This is because self-exciting point processes like MHP explicitly model the mutually exciting and decaying patterns of the video’s popularity dynamics. This proves that capturing the nuanced event-driven cascade is essential for creating a high-fidelity temporal representation.

Finally, the modality ablation (Table 2, Bottom Right) isolating the retrieved label, visual content, audio, and text demonstrates that multi-modal fusion is highly valuable. Each individual modality contributes positively to the overall predictive accuracy. Notably, even with the ablation of retrieved labels, the model maintains strong performance and still outperforms other baselines. This underscores that effectively combining temporal event trajectories with multi-modal video content is a fundamentally sound approach to popularity prediction.

4.5 Complexity Discussion and Practicality

Our architecture is strategically designed around a two-phase process: a one-time, computationally intensive **offline stage** for building a retrieval-ready memory bank, and a highly efficient **online stage** for real-time inference.

Offline Memory Bank Construction. This phase involves processing each of the videos in the historical corpus. The key operations include computationally expensive feature extractions, such as multi-modal feature extraction (i.e., ViT, AST), MHP temporal embedding generation, and unified retrieval vector creation (i.e.,

Prediction	noTemp	noRet	noMHP	M ³ TR	Temporal	nMSE	SRC	MAE
Top50	75.000	77.908	71.688	88.030	None	0.741	0.529	23.81
Top200	57.690	56.513	55.616	64.266	Pad&Mask	0.800	0.506	24.36
Top500	43.111	44.420	41.604	44.443	Poisson	0.765	0.525	24.02
Bottom500	27.714	26.017	26.339	25.866	Neural HP	0.723	0.537	23.44
Bottom200	22.638	22.544	22.818	22.447	Mamba HP	0.705	0.559	23.10
Bottom50	23.409	22.414	19.536	22.183	Ablation	nMSE	SRC	MAE
					w/o label	0.746	0.506	24.76
nMSE(↓)	0.7413	0.7980	0.8002	0.7051	w/o audio	0.739	0.525	23.53
SRC(↑)	0.5286	0.5047	0.5064	0.5587	w/o visual	0.735	0.519	23.49
MAE(↓)	23.814	25.198	24.359	23.097	w/o text	0.718	0.534	23.37
					with all	0.705	0.559	23.10

Table 2: Comprehensive ablation study results demonstrating the effectiveness of the proposed components in M³TR. Left: Ablation among four primary variants (noTemporal, noRetrieval, noMHP, and M³TR) evaluated across different popularity rank groupings (Top/Bottom) and overall metrics. The results indicate that our full M³TR framework yields the most robust predictions across both highly popular (head) and less popular (tail) videos. Top Right: Performance comparison of different temporal modeling strategies. It highlights the superiority of the Mamba Hawkes Process (MHP) in capturing the mutually exciting and decaying patterns of user event cascades compared to simpler baselines like Padding&Masking or Poisson Process. Bottom Right: Modality ablation isolating the retrieved label, visual content, audio, and text. This confirms that multi-modal fusion is highly valuable, with each individual modality contributing positively to the overall predictive accuracy.

BLIP-2, CLAP). To contextualize the computational cost, we processed nearly 20,000 samples using four RTX 3090 GPUs. The initial visual and acoustic captioning take 398 and 182 minutes, respectively. Following this, the Temporal Embedding is completed in 13 minutes, while the Textual, Visual, and Acoustic Embeddings require 8, 33 and 146 minutes, respectively. Finally, the Unified Alignment Embedding (UAE) processing concludes in just 5 minutes. These features are generated only once per video and stored in an efficient Approximate Nearest Neighbor (ANN) search index. For our experiments, we utilized FAISS with a [e.g., IVF1024, PQ64] index [10, 20, 23], which balances search speed and memory. The total cost scales linearly with video number and can be distributed across a compute cluster. Once the offline pre-processing is complete, the entire model is trained in merely 24 minutes.

Online Real-Time Inference. When a new video requires a prediction, the latency is critical, and our trained model is fully capable of real-time inference. The online inference stage is engineered for low-latency performance. Following the feature extraction for the target video, we leverage Approximate Nearest Neighbor search algorithms, e.g., FAISS [22], to reduce retrieval complexity to a highly scalable $O(\log N_{\text{bank}})$. Subsequently, the final fusion module operates only on the small, retrieved set of S exemplars. Its complexity is therefore a low constant, roughly $O(S \cdot d^2)$, and is crucially independent of the memory bank size. This design ensures the entire online prediction pipeline is efficient and scalable for real-world deployment. A more detailed, real-time breakdown of these components is provided in Appendix [H](#).

5 Conclusion

In this work, we introduce M³TR, a framework that establishes a new SOTA in MVPP. Our central contribution is the insight that a video’s underlying temporal archetype is as critical as its content for long-term forecasting. We address the limitations of prior art by synergizing two core innovations: (1) a Mamba-Hawkes Process that captures the intricate, self-exciting nature of user interactions, and (2) a temporal-aware retrieval mechanism that identifies historical videos based on both content and dynamic patterns. Our results validate that retrieving videos with similar popularity trajectories provides more robust signals for forecasting than content similarity alone.

Acknowledgments

This work was supported by the Shanghai Jiao Tong University under “Bo Le” Grant AO120001/074.

References

- [1] Khushnood Abbas, Mohammad Kamrul Hasan, Alireza Abbasi, Shi Dong, Taher M. Ghazal, Siti Norul Huda Sheikh Abdullah, Asif Khan, Dabiah Alboaneen, Fatima Rayan Awad Ahmed, Thowiba E. Ahmed, and Shayla Islam. 2023. Co-Evolving Popularity Prediction in Temporal Bipartite Networks: A Heuristics Based Model. *IEEE Access* 11 (2023), 37546–37559.
- [2] Fatma S. Abousaleh, Wen-Huang Cheng, Neng-Hao Yu, and Yu Tsao. 2021. Multimodal Deep Learning Framework for Image Popularity Prediction on Social Media. *IEEE Transactions on Cognitive and Developmental Systems* 13, 3 (2021), 679–692.
- [3] Jingyuan Chen, Xuemeng Song, Liqiang Nie, Xiang Wang, Hanwang Zhang, and Tat-Seng Chua. 2016. Micro Tells Macro: Predicting the Popularity of Micro-Videos via a Transductive Model. In *Proceedings of the 24th ACM International Conference on Multimedia (MM)*.
- [4] Shuai Chen, Gerda Bortsova, Antonio García-Uceda Juárez, Gijs Van Tulder, and Marleen De Bruijne. 2019. Multi-task attention-based semi-supervised learning for medical image segmentation. In *International Conference on Medical Image Computing and Computer Assisted Intervention (MICCAI)*.
- [5] Yuanda Chen. 2016. Thinning algorithms for simulating point processes. *Florida State University, Tallahassee, FL* (2016).
- [6] Zhangtao Cheng, Jienan Zhang, Xovee Xu, Goce Trajcevski, Ting Zhong, and Fan Zhou. 2024. Retrieval-Augmented Hypergraph for Multimodal Social Media Popularity Prediction. In *Proceedings of the 30th ACM SIGKDD Conference on Knowledge Discovery and Data Mining (SIGKDD)*.
- [7] Tsun-hin Cheung and Kin-man Lam. 2022. Crossmodal Bipolar Attention for Multimodal Classification on Social Media. *Neurocomputing* 514 (2022), 1–12.
- [8] Minhwa Cho, Dahye Jeong, and Eunil Park. 2024. AMPS: Predicting popularity of short-form videos using multi-modal attention mechanisms in social media marketing environments. *Journal of Retailing and Consumer Services* 78 (2024), 103778.
- [9] Alexey Dosovitskiy. 2020. An Image is Worth 16x16 Words: Transformers for Image Recognition at Scale. *arXiv preprint arXiv:2010.11929* (2020).
- [10] Matthijs Douze, Alexandr Guzhva, Chengqi Deng, Jeff Johnson, Gergely Szilvasy, Pierre-Emmanuel Mazaré, Maria Lomeli, Lucas Hosseini, and Hervé Jégou. 2024. The Faiss library. *arXiv preprint arXiv:2401.08281* (2024).
- [11] Mor Geva, Roei Schuster, Jonathan Berant, and Omer Levy. 2020. Transformer Feed-Forward Layers Are Key-Value Memories. *arXiv preprint arXiv:2012.14913* (2020).
- [12] Shalini Ghosh, Oriol Vinyals, Brian Strope, Scott Roy, Tom Dean, and Larry Heck. 2016. Contextual LSTM (CLSTM) models for Large scale NLP tasks. *arXiv preprint arXiv:1602.06291* (2016).
- [13] Yuan Gong, Yu-An Chung, and James Glass. 2021. AST: Audio spectrogram transformer. In *Proc. Interspeech*.
- [14] Yuan Gong, Yu-An Chung, and James Glass. 2021. Ast: Audio spectrogram transformer. *arXiv preprint arXiv:2104.01778* (2021).
- [15] Albert Gu and Tri Dao. 2023. Mamba: Linear-Time Sequence Modeling with Selective State Spaces.
- [16] Ruiqi Guo, Quan Geng, David Simcha, Felix Chern, Sanjiv Kumar, and Xiang Wu. 2019. New Loss Functions for Fast Maximum Inner Product Search. *ArXiv* (2019).
- [17] Firoz Hasan, Dewan Mamun Raza, Hasan Moon, and Md Aynul Hasan Nahid. 2023. Sentiment Analysis from YouTube Video Using Bi-LSTM-GRU Classification. In *International Conference on Big Data, IoT and Machine Learning (BLM)*.

- [18] Zichen He and Danian Li. 2024. The Short Video Popularity Prediction Using Internet of Things and Deep Learning. *IEEE Access* 12 (2024), 47508–47517.
- [19] Amin Javari and Mahdi Jalili. 2014. Accurate and Novel Recommendations: An Algorithm Based on Popularity Forecasting. *ACM Transactions on Intelligent Systems and Technology* 5, 4 (2014), 1–20.
- [20] Hervé Jégou, Matthijs Douze, and Cordelia Schmid. 2011. Product quantization for nearest neighbor search. *IEEE transactions on pattern analysis and machine intelligence* 33, 1 (2011), 117–128.
- [21] Peiguang Jing, Yuting Su, Liqiang Nie, Xu Bai, Jing Liu, and Meng Wang. 2017. Low-Rank Multi-View Embedding Learning for Micro-Video Popularity Prediction. *IEEE Transactions on Knowledge and Data Engineering* 30, 8 (2017), 1519–1532.
- [22] Jeff Johnson, Matthijs Douze, and Hervé Jégou. 2017. Billion-Scale Similarity Search with GPUs. *IEEE Transactions on Big Data* (2017).
- [23] Jeff Johnson, Matthijs Douze, and Hervé Jégou. 2019. Billion-scale similarity search with GPUs. *IEEE Transactions on Big Data* 7, 3 (2019), 535–547.
- [24] Donald R Jones, Matthias Schonlau, and William J Welch. 1998. Efficient Global Optimization of Expensive Black-Box Functions. 455–492 pages.
- [25] Aditya Khosla, Atish Das Sarma, and Raffay Hamid. 2014. What Makes an Image Popular?. In *Proceedings of the 23rd International Conference on World Wide Web (WWW)*.
- [26] Xin Lai, Yihong Zhang, and Wei Zhang. 2020. Hyfea: Winning Solution to Social Media Popularity Prediction For Multimedia Grand Challenge 2020. In *Proceedings of the 28th ACM International Conference on Multimedia (MM)*.
- [27] Himabindu Lakkaraju and Jitendra Ajmera. 2011. Attention Prediction On Social Media Brand Pages. In *Proceedings of the 20th ACM International Conference on Information and Knowledge Management (CIKM)*.
- [28] Hannes Leeb and Benedikt M Pötscher. 2008. Sparse estimators and the oracle property, or the return of Hodges’ estimator. *Journal of Econometrics* 142, 1 (2008), 201–211.
- [29] Junnan Li, Dongxu Li, Silvio Savarese, and Steven Hoi. 2023. BLIP-2: Bootstrapping Language-Image Pre-training with Frozen Image Encoders and Large Language Models. In *International Conference on Machine Learning (ICML)*.
- [30] Xianming Li and Jing Li. 2024. AoE: Angle-optimized embeddings for semantic textual similarity. In *Proceedings of the 62nd Annual Meeting of the Association for Computational Linguistics (ACL)*.
- [31] Jiacheng Lu, Mingyuan Xiao, Weijian Wang, Yuxin Du, Zhengze Wu, and Cheng Hua. 2025. Multi-modal and Metadata Capture Model for Micro Video Popularity Prediction. *arXiv preprint arXiv:2502.17038* (2025).
- [32] Yongxin Ni, Yu Cheng, Xiangyan Liu, Junchen Fu, Youhua Li, Xiangnan He, Yongfeng Zhang, and Fajie Yuan. 2023. A Content-driven Micro-video Recommendation Dataset at Scale. *arXiv preprint arXiv:2309.15379* (2023).
- [33] Meher UN Nisa, Danish Mahmood, Ghufuran Ahmed, Suleman Khan, Mazin Abed Mohammed, and Robertas Damaševičius. 2021. Optimizing prediction of YouTube video popularity using XGBoost. *Electronics* 10, 23 (2021), 2962.
- [34] Henri J Nussbaumer and Henri J Nussbaumer. 1982. *The fast Fourier transform*. Springer.
- [35] Sandipan Sahu, Raghvendra Kumar, Mohd Shafi Pathan, Jana Shafi, Yogesh Kumar, and Muhammad Fazal Ijaz. 2022. Movie Popularity and Target Audience Prediction Using the Content-Based Recommender System. *IEEE Access* 10 (2022), 42044–42060.
- [36] Robert H Shumway, David S Stoffer, Robert H Shumway, and David S Stoffer. 2017. ARIMA models. *Time series analysis and its applications: with R examples* (2017), 75–163.
- [37] Xiaobing Sun and Wei Lu. 2020. Understanding Attention for Text Classification. In *Proceedings of the 58th Annual Meeting of the Association for Computational Linguistics (ACL)*.
- [38] Yusong Wu, Ke Chen, Tianyu Zhang, Yuchen Hui, Taylor Berg-Kirkpatrick, and Shlomo Dubnov. 2023. Large-scale Contrastive Language-Audio Pretraining with Feature Fusion and Keyword-to-Caption Augmentation. In *IEEE International Conference on Acoustics, Speech and Signal Processing (ICASSP)*.
- [39] Jiayi Xie, Yaochen Zhu, and Zhenzhong Chen. 2023. Micro-Video Popularity Prediction Via Multimodal Variational Information Bottleneck. *IEEE Transactions on Multimedia* (2023).
- [40] Haoran Xu, Mengduo Yang, Jie Zhou, and Jiaye Li. 2024. Short-form UGC Video Quality Assessment Based on Multi-Level Video Fusion with Rank-Aware. In *IEEE/CVF Conference on Computer Vision and Pattern Recognition Workshops (CVPRW)*.
- [41] Jie Xu, Mihaela van der Schaar, Jiangchuan Liu, and Haitao Li. 2015. Forecasting Popularity of Videos Using Social Media. *IEEE Journal of Selected Topics in Signal Processing* 9, 2 (2015), 330–343.
- [42] Cun-Hui Zhang. 2010. Nearly unbiased variable selection under minimax concave penalty. *Annals of Statistics* (2010).
- [43] Jinghui Zhang, Mochen Yang, Xuan Bi, and Qiang Wei. 2024. Algorithmic Governance via Recommender Systems: The Case of Short Video Platform. Available at SSRN 4572513 (2024).
- [44] Lu-Tao Zhao, Yue Li, Xue-Hui Chen, Liu-Yi Sun, and Ze-Yu Xue. 2024. MFTM-Informer: A multi-step prediction model based on multivariate fuzzy trend matching and Informer. *Information Sciences* 681 (2024), 121268.
- [45] Ting Zhong, Jian Lang, Yifan Zhang, Zhangtao Cheng, Kunpeng Zhang, and Fan Zhou. 2024. Predicting Micro-video Popularity via Multi-modal Retrieval Augmentation. In *Proceedings of the 47th International ACM SIGIR Conference on Research and Development in Information Retrieval (SIGIR)*.

Appendix

A More Challenges Faced by Previous Methods

Current micro-video popularity prediction research suffers from two main limitations, demonstrable through analysis of the MicroLens-50k dataset [32] and visualized in Figures 1. First, existing models lack a comprehensive understanding of user interests. While some approaches focus on temporal user feedback (likes, comments, shares, etc.), few effectively integrate these with retrieval mechanisms. This prevents models from capturing contextualized user interests. For example, retrieval methods relying solely on user behavior similarity often fail to distinguish between videos with similar initial popularity but diverging later trends, as illustrated in Figure 1b (the “initial rise, then decline” scenario). These methods don’t adequately connect content and dynamic feedback (e.g., increasing negative comments) to accurately reflect the changing user interest. Furthermore, fine-grained interest understanding, like differentiating user preferences for various video modalities, is often neglected.

Second, existing models, including retrieval-based ones, show deficiencies in accuracy, robustness, cold-start handling, and adaptability. Insufficient information use and limitations in retrieval (e.g., susceptibility to noise, as shown in Figure 1c for the “noise interference” scenario) lead to prediction biases. While retrieval-based models generally outperform feature-engineering and user-behavior/deep-learning models in scenarios with consistent positive feedback (Figure 1c, “positive feedback” scenario), analysis of MicroLens-50k data reveals that all model types struggle with contextualized interests, noise, and cold-start situations (sparse early feedback). This is evident across all scenarios, including the steady growth scenario in Figure 1a, where even the best-performing retrieval-based models show some deviation from perfect prediction. This highlights the critical need for a more effective integration of multi-modal information and temporal user feedback within the retrieval framework to improve prediction accuracy and robustness, especially in more complex situations like those depicted in Figures 1b and 1c.

To contextualize the challenges inherent in Micro-Video Popularity Prediction (MVPP), it is crucial to first appreciate the sheer diversity of engagement trajectories that videos exhibit over their lifecycle. The assumption of a single, uniform growth model is untenable, as different videos possess fundamentally distinct temporal signatures. A predictive model that fails to account for this diversity is bound to have limited real-world applicability. Figure 2 provides a qualitative illustration of four common yet disparate popularity archetypes, underscoring the necessity for a sophisticated model capable of understanding and forecasting these complex temporal dynamics.

“Viral Explosion” is characterized by a steep, exponential accumulation of engagement within a very short timeframe. These videos achieve peak popularity rapidly before the growth rate saturates. “Slow Burn” exhibits a more gradual but sustained growth in popularity. These videos accumulate engagement at a steady, often linear, rate over a much longer period, lacking the initial explosive phase. “Flash in the Pan” (Early Surge, Later Decline) represents a particularly challenging scenario where a video shows strong initial promise but fails to maintain momentum. User interest or relevance

wanes, leading to a premature plateau or even a decline in the rate of new engagement. And “Sleeper Hit” represents that these videos remain dormant with minimal engagement for an initial period before a delayed catalyst (e.g., a mention and a change in algorithm) triggers a sudden and often rapid rise in popularity.

The existence of these disparate “temporal DNAs” is the central challenge that our work addresses. Two videos with nearly identical multi-modal content features could follow entirely different paths; for example, one might become a “Viral Explosion” while the other is a “Flash in the Pan”. This observation strongly motivates our core hypothesis: a successful prediction framework must look beyond static content similarity and develop a deep, nuanced understanding of a video’s temporal signature. The M³TR framework, particularly with its Mamba-Hawkes Process (MHP) module, is specifically designed to model these intricate event dynamics. Furthermore, our temporal-aware retrieval mechanism is engineered to identify historically relevant examples that share a similar temporal DNA, providing the crucial context that content-only models invariably miss.

B Mamba Architecture

We begin with the continuous form of the classic State Space Models (SSM), gradually introducing how to discretize them, implement input-dependent dynamics, and optimize for parallel scan on GPUs for efficient training and inference.

B.1 Intro: From Traditional Transformers to Mamba

Transformers and their self-attention mechanism have shown exceptional performance across various sequence tasks, such as natural language, genomics, and audio signals. However, the self-attention module in Transformer models exhibits a quadratic time and memory complexity with respect to the sequence length L , making them prohibitively expensive for long sequences. Several alternatives to address this inefficiency have been proposed, including:

- **Linear Attention:** Using kernel methods or approximations to reduce the attention complexity to linear, though still not matching the performance of full attention in certain dense information settings like natural language modeling.
- **Gated Convolutions and RNN-based models:** Examples like Gated CNN and LSTM that improve local feature modeling or long-range dependencies but often underperform compared to attention models in large-scale data or complex tasks.
- **Structured State Space Models (SSMs):** Models like S4, S5, and H3 utilize specific structural assumptions for the state transition matrix A , allowing for parallelizable convolutions and efficient modeling of long sequences. However, they struggle in discrete, information-dense input domains such as text.

Mamba’s introduction is driven by a core innovation: **introducing a selective mechanism into the SSM**, where the parameters of the state space model dynamically depend on the input, allowing the model to propagate or forget information based on the current input context. This design retains the SSM’s ability to efficiently

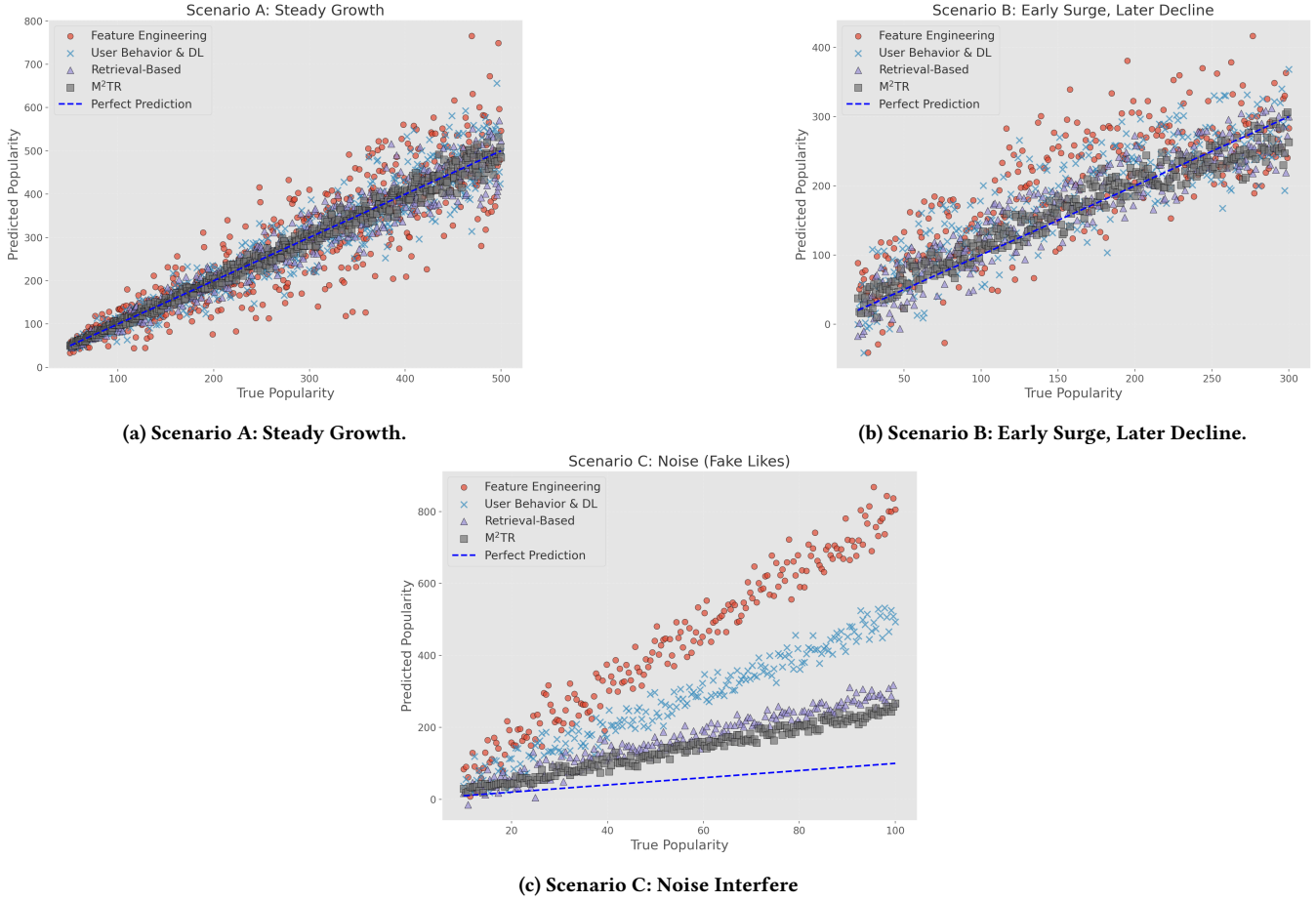


Figure 1: Comparisons of Different Scenarios of Video Popularity Trends. (a) Steady growth, (b) Early surge with later decline, (c) Noise from fake likes.

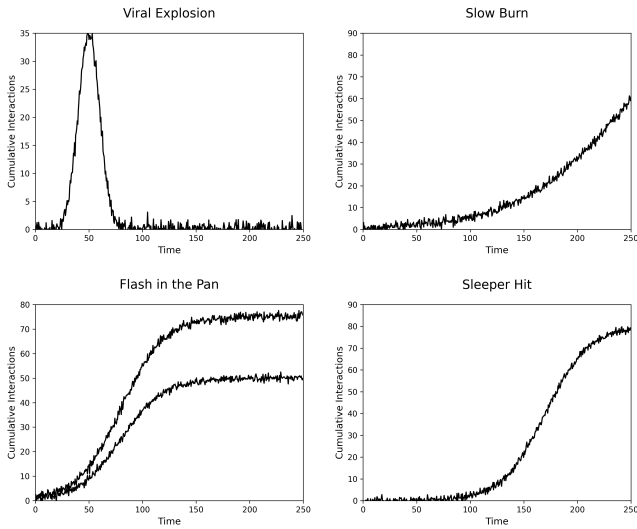


Figure 2: Diversity of Micro-Video Popularity Trajectories

model long-range dependencies while addressing the shortcomings of existing methods for discrete tasks.

B.2 Continuous-Time State Space Models Overview

B.2.1 Continuous Form. A classic (linear) state space model is described by the following continuous differential equations:

$$\begin{cases} \dot{\mathbf{h}}(t) = \mathbf{A}\mathbf{h}(t) + \mathbf{B}\mathbf{x}(t), \\ \mathbf{y}(t) = \mathbf{C}\mathbf{h}(t), \end{cases} \quad (1)$$

where $\mathbf{h}(t) \in \mathbb{R}^N$ is the state vector of the system at time t ; $\mathbf{x}(t) \in \mathbb{R}$ is the input (the formulation can be extended to multi-channel inputs $\mathbf{x}(t) \in \mathbb{R}^d$); $\mathbf{y}(t) \in \mathbb{R}$ is the output (again extendable to multi-channel); $\mathbf{A} \in \mathbb{R}^{N \times N}$, $\mathbf{B} \in \mathbb{R}^{N \times 1}$, $\mathbf{C} \in \mathbb{R}^{1 \times N}$ are the state transition, input projection, and output projection matrices, respectively.

Under the assumption of **Linear Time-Invariance (LTI)**, the matrices \mathbf{A} , \mathbf{B} , and \mathbf{C} are time-invariant. However, when extended to **Linear Time-Varying (LTV)** systems, these matrices can depend on time, enabling more flexible modeling. Mamba pushes beyond

the traditional SSM by introducing input-dependent parameters, which we call **selectivity**.

B.2.2 Discretization Process. In practical applications, continuous-time state space models need to be discretized. The following outlines the discretization process using Zero-Order Hold (ZOH) approximation. Assuming that $\mathbf{x}(t)$ remains constant over the interval $[k\Delta t, (k+1)\Delta t]$, we discretize the state update equation:

$$\begin{aligned} \mathbf{h}[k+1] &= e^{A\Delta t}\mathbf{h}[k] + \int_0^{\Delta t} e^{A(\Delta t-\tau)} d\tau \mathbf{B}\mathbf{x}[k], \\ \mathbf{y}[k] &= \mathbf{C}\mathbf{h}[k]. \end{aligned} \quad (2)$$

By approximating the integral and simplifying, we arrive at:

$$\mathbf{h}[k+1] = \bar{\mathbf{A}}\mathbf{h}[k] + \bar{\mathbf{B}}\mathbf{x}[k], \quad \mathbf{y}[k] = \mathbf{C}\mathbf{h}[k], \quad (3)$$

where $\bar{\mathbf{A}} = e^{A\Delta t}$ and $\bar{\mathbf{B}} = A^{-1}(e^{A\Delta t} - \mathbf{I})\mathbf{B}$.

This discretized form is more suitable for digital computation, especially in sequence modeling tasks.

B.3 From SSM to Selective SSM (SSSM)

B.3.1 Principle and Motivation. In standard SSMs (LTI), $\bar{\mathbf{A}}, \bar{\mathbf{B}}, \mathbf{C}$ remain time-invariant, effectively making the system equivalent to a fixed convolution or linear recurrence. This property allows for efficient computation using FFT (when the sampling rate is fixed) or online recurrent scans, achieving $O(L \log L)$ complexity. However, in tasks such as natural language modeling, where the input consists of discrete tokens, it is difficult for these models to “selectively” retain or forget certain parts of the input sequence without introducing inefficiencies.

Selective SSM (SSSM) introduces input-dependent dynamics into the model, allowing the state transition matrices $\bar{\mathbf{A}}, \bar{\mathbf{B}}, \mathbf{C}$ to vary with the current input $\mathbf{x}[k]$:

$$\begin{cases} \mathbf{h}[k+1] = \bar{\mathbf{A}}(\mathbf{x}[k])\mathbf{h}[k] + \bar{\mathbf{B}}(\mathbf{x}[k])\mathbf{x}[k], \\ \mathbf{y}[k] = \mathbf{C}(\mathbf{x}[k])\mathbf{h}[k]. \end{cases} \quad (4)$$

At each step k , the model computes a set of “selective” or “gated” parameters based on $\mathbf{x}[k]$, which are then used to update the state $\mathbf{h}[k]$ and produce the output $\mathbf{y}[k]$. This allows the model to focus on or forget particular inputs based on their relevance to the current context.

B.3.2 Specific Forms of Input-Dependent Parameters. In practice, it is common to define the input-dependent parameters $\bar{\mathbf{B}}(\mathbf{x}[k])$, $\mathbf{C}(\mathbf{x}[k])$, and $\Delta(\mathbf{x}[k])$ using a parameterized function, such as:

$$\bar{\mathbf{B}}(\mathbf{x}[k]) = \text{Linear}_N(\mathbf{x}[k]), \quad \mathbf{C}(\mathbf{x}[k]) = \text{Linear}_N(\mathbf{x}[k]), \quad (5)$$

$$\Delta(\mathbf{x}[k]) = \text{Broadcast}_D(\text{Linear}_1(\mathbf{x}[k])). \quad (6)$$

This input-dependent design makes the model more expressive, enabling selective memory and forgetting of sequence elements. The dynamic parameterization of Δ is similar to gating mechanisms in RNNs (such as in LSTM), but with a more flexible, input-driven mechanism that adjusts how much of the previous state is retained.

B.4 Mamba Architecture Implementation Details

The Mamba architecture integrates the aforementioned selective SSM as its core sequence transformation block, combining it with a simplified gated MLP layer to form a unified network module. Unlike the traditional “attention + MLP” stacked blocks (e.g., Transformer blocks) or the “SSM + MLP” alternations (e.g., H3 architecture), Mamba uses a **homogeneous** design: it combines SSSM with MLP gating directly in the main branch and stacks them in each layer (or block) of the network.

The structure of the Mamba block includes:

- **Projection Layer:** Linearly transforms the input channels to a higher dimension (controlled by an expansion ratio).
- **Non-linearity / Gating:** A multiplicative or additive gating function is applied to the higher-dimensional representation, using activations such as SiLU, Swish, or Sigmoid.
- **Selective SSM:** The gated representation is passed through the selective SSM block, performing sequence-wise integration and long-range modeling.
- **Output Projection Layer:** Projects the high-dimensional representation back to the original number of channels.

All these layers are stacked in the sequence dimension, forming the full network architecture. Empirical experiments show that this design performs exceptionally well across tasks involving text (discrete tokens), audio (continuous signals), and genomic sequences (long and discrete sequences).

B.5 Parallel Scan and Hardware Optimization

B.5.1 Why Not Use FFT or Convolutions. In traditional LTI SSMs (e.g., S4), the state recurrence can be unfolded as a global convolution, allowing for FFT-based acceleration, achieving near $O(L \log L)$ complexity. However, in selective SSMs, the input-dependent dynamics ($\bar{\mathbf{A}}(k), \bar{\mathbf{B}}(k)$) break the time invariance, making direct use of convolutions or FFT infeasible.

B.5.2 Parallel Scan Algorithm and Memory Hierarchy. To address this issue, Mamba utilizes a hardware-friendly parallel scan algorithm to update the states in a recurrent computation mode. The key idea is:

- **Chunking:** The long sequence is divided into smaller chunks, each of which can be processed in parallel on the GPU, reducing global sequential dependencies.
- **Prefix / Suffix Merging:** Similar to prefix sum computation, the model computes local states within each chunk first, and then merges them using a tree-like structure (in “upsweep” and “downsweep”).
- **Memory Management:** Most parameters (e.g., $\bar{\mathbf{A}}, \bar{\mathbf{B}}, \mathbf{C}, \Delta$) are stored in the GPU’s high-bandwidth memory (HBM), but only the necessary data from the current chunk is loaded into faster on-chip memory (SRAM or shared memory) for computation, minimizing memory bandwidth bottlenecks.

This approach significantly accelerates the computation by reducing the memory overhead and enabling more parallelism.

B.5.3 Complexity Comparison.

- **Time Complexity:** Mamba achieves an ideal time complexity of $O(NLd)$ (where N is the hidden state dimension, and d is the input-output channel size), compared to the $O(L \log L)$ complexity of convolution-based methods. This makes it more advantageous for very long sequences, especially in GPU-parallel environments.
- **Space Complexity:** Through chunking and recomputation techniques, the memory usage is reduced to $O(\text{batch size} \times d \times \text{chunk size})$, making it scalable for long sequences.

C Classical Hawkes Processes: A Detailed Exposition

C.1 Preliminaries: Counting and Point Processes

We begin by formally defining the foundational concepts of counting and point processes.

Definition C.1 (Counting Process). A stochastic process $\{N(t), t \geq 0\}$ is defined as a **counting process** if it satisfies the following conditions:

- $N(0) = 0$ almost surely (a.s.). This signifies that the counting process begins with no observed events.
- $N(t) \in \{0, 1, 2, \dots\}$ for all $t \geq 0$. The process only takes on non-negative integer values, representing the number of events that have occurred.
- If $s < t$, then $N(s) \leq N(t)$ a.s. The process is non-decreasing; the number of events can only increase or remain the same.
- $N(t) - N(s)$ represents the number of events that occur in the time interval $(s, t]$.
- $N(t)$ is right-continuous with left limits (rcll or cadlag). This means that $N(t) = \lim_{s \rightarrow t^+} N(s)$ and the left limit $\lim_{s \rightarrow t^-} N(s)$ exists. Right-continuity ensures that the counting process includes events at the right endpoint.
- The process increases by jumps of size +1. Each event increments the counter by exactly one.

Definition C.2 (Point Process). A **point process** is a random sequence of points (or events) $\{T_i\}_{i=1}^{\infty}$ in time, where $0 < T_1 < T_2 < \dots < \infty$ a.s.

- T_i denotes the time of the i -th event occurrence.
- The point process is assumed to be simple, meaning no two events occur at the same time, i.e., $T_i \neq T_j$ for $i \neq j$.
- It is common to define $T_0 = 0$ for convenience, even though this event isn't counted by the counting process.

Definition C.3 (Relationship: Counting & Point Processes). The counting process $N(t)$ can be constructed from the point process $\{T_i\}_{i=1}^{\infty}$ as follows:

$$N(t) = \sum_{i=1}^{\infty} \mathbb{I}(T_i \leq t) = \sum_{T_i \leq t} 1, \quad (7)$$

where $\mathbb{I}(A)$ is the indicator function, equal to 1 if event A occurs and 0 otherwise. This essentially counts the number of events T_i that have occurred up to time t .

Definition C.4 (Inter-Arrival Times). The inter-arrival times $\{E_i\}_{i=1}^{\infty}$ are defined as $E_i = T_i - T_{i-1}$ for $i \geq 1$, with $T_0 = 0$. Inter-arrival times represent the time between consecutive events.

Example C.5 (Homogeneous Poisson Process). The simplest example of a counting process is the **homogeneous Poisson process** with rate $\lambda > 0$. In this case, the inter-arrival times are independent and identically distributed (i.i.d.) exponential random variables: E_i i.i.d. $\text{Exponential}(\lambda)$. This means:

- The probability density function (pdf) of each E_i is given by $f_{E_i}(x) = \lambda e^{-\lambda x}$ for $x \geq 0$.
- The expected value of each inter-arrival time is $\mathbb{E}[E_i] = \frac{1}{\lambda}$.
- The expected number of events per unit time is $\mathbb{E}\left[\frac{N(t)}{t}\right] = \lambda$. This means that the long-run average rate of event occurrence is λ .

C.2 Conditional Intensity and Compensator

These concepts provide a fundamental way to characterize point processes and their dependence on their past history.

Definition C.6 (Filtration). Let $(\Omega, \mathcal{F}, \mathbb{P})$ be a probability space. A **filtration** $\{\mathcal{H}_t\}_{t \geq 0}$ is a family of σ -algebras such that:

- $\mathcal{H}_t \subseteq \mathcal{F}$ for all $t \geq 0$. Each \mathcal{H}_t contains information about events that are measurable in the original probability space.
- $\mathcal{H}_s \subseteq \mathcal{H}_t$ for all $0 \leq s \leq t$. The information available increases (or stays the same) as time progresses.

Intuitively, \mathcal{H}_t represents all the information known about the process up to time t .

Definition C.7 (History of a Counting Process). The **history** of a counting process $\{N(t), t \geq 0\}$, denoted as $\{\mathcal{H}_t\}_{t \geq 0}$, is the filtration generated by the process:

$$\mathcal{H}_t = \sigma(\{N(s) : 0 \leq s < t\}). \quad (8)$$

This means \mathcal{H}_t contains all information about the path of the process $N(s)$ for all times s strictly less than t . Note the strict inequality.

Definition C.8 (Conditional Intensity Process). The **conditional intensity process** of a counting process $N(t)$ is defined as

$$\lambda^*(t) = \lim_{\Delta \rightarrow 0} \frac{\mathbb{E}(N_{t+\Delta} - N_t \mid \mathcal{H}_t)}{\Delta}, \quad (9)$$

if this limit exists. This limit represents the instantaneous rate of event occurrence at time t , given the history of the process up to (but not including) time t .

Alternatively, we can write:

$$\mathbb{P}(dN(t) = 1 \mid \mathcal{H}_t) = \lambda^*(t)dt + o(dt), \quad (10)$$

where $dN(t) = N(t + dt) - N(t)$ and $o(dt)$ is a term that goes to zero faster than dt as $dt \rightarrow 0$.

Remark 1. It is crucial to note that $\lambda^*(t)$ is generally a stochastic process itself, reflecting the fact that the rate of event occurrence can change randomly over time based on the history. The superscript $*$ is used to emphasize its random nature. The conditional intensity is typically left-continuous with right limits (lclr or caglad).

Example C.9 (Poisson Process and Conditional Intensity). If the conditional intensity process $\lambda^*(t) \equiv \lambda(t)$ is a deterministic function of time, meaning it doesn't depend on the history \mathcal{H}_t , then the counting process $N(t)$ is a **Poisson process** with rate function $\lambda(t)$. If $\lambda(t) \equiv \lambda$ is a constant (independent of time), then it is a **homogeneous Poisson process**.

Definition C.10 (Compensator). The **compensator** of a point process $N(t)$ is defined as

$$\Lambda_t = \int_0^t \lambda^*(s) ds. \quad (11)$$

The compensator represents the expected cumulative number of events up to time t , given the history of the process.

THEOREM C.11 (MARTINGALE CHARACTERIZATION OF THE COMPENSATOR). *The compensator Λ_t uniquely characterizes the point process $N(t)$. Specifically, Λ_t is the unique predictable process for which the difference*

$$M_t = N_t - \Lambda_t \quad (12)$$

is a local martingale with respect to the filtration \mathcal{H}_t . This means that

- $\mathbb{E}[|M_t|] < \infty$ for all $t \geq 0$.
- $\mathbb{E}[M_t | \mathcal{H}_s] = M_s$ for all $0 \leq s \leq t$.

M_t represents a “fair game”, where the expected future value, given past information, is equal to the current value. The compensator removes the predictable part of the process, leaving only the random, unpredictable component.

Remark 2. If Λ_t is absolutely continuous with respect to t , its pathwise derivative is $\lambda^*(t)$, recovering the conditional intensity interpretation. Moreover, $N(t)$ is a Poisson process if and only if Λ_t is a deterministic function of t .

C.3 The Hawkes Process: Definition and Self-Excitation

We now define the Hawkes process, highlighting its key property of self-excitation.

Definition C.12 (Hawkes Process). A **Hawkes process** is a counting process $\{N(t), t \geq 0\}$ whose conditional intensity process is given by

$$\lambda^*(t) = \lambda + \sum_{T_i < t} \mu(t - T_i), \quad (13)$$

where:

- $\lambda > 0$ is the **background arrival rate**. This represents the baseline rate of events occurring independently of past events.
- $\mu : \mathbb{R}_+ \rightarrow \mathbb{R}_+$ is the **excitation function** or **kernel**. This function determines how past events influence the current intensity.

The excitation function $\mu(t)$ is the cornerstone of self-excitation. It quantifies the increase in the intensity process at time t due to an event that occurred at time $T_i < t$.

Definition C.13 (Self-Excitation). The property of **self-excitation** in a Hawkes process arises because the occurrence of an event at time T_i instantaneously increases the conditional intensity $\lambda^*(t)$ for $t > T_i$ by an amount determined by the excitation function $\mu(t - T_i)$. This increase in intensity makes subsequent events more likely to occur in the near future, leading to clustering of events.

Example C.14 (Exponentially Decaying Hawkes Process). A common and analytically tractable choice for the excitation function is the exponentially decaying kernel:

$$\mu(t) = \alpha e^{-\beta t}, \quad (14)$$

where $\alpha > 0$ controls the magnitude of the excitation, and $\beta > 0$ controls the rate of decay of the excitation. This means that the influence of past events diminishes exponentially over time.

C.4 Non-homogeneous Poisson Process and Thinning Algorithm

Non-homogeneous Poisson Process and Ogata’s Thinning Algorithm as follows:

Algorithm 1 Ogata’s Thinning Algorithm for Non-homogeneous Poisson Process

Input: Intensity function $\lambda_k(t)$, start time T_{orig} , end time T_{end}

Output: Padded event sequence $\mathcal{T}_{\text{pad}}^{(k)} = \{t_{\text{pad}}^{(1)}, \dots, t_{\text{pad}}^{(N_k)}\}$

1: **Step 1: Determine an Upper Bound**

2: Find a constant $\lambda_{\text{max}}^{(k)}$ such that $\lambda_k(t) \leq \lambda_{\text{max}}^{(k)}$ for all $t \in [T_{\text{orig}}, T_{\text{end}}]$

3: **Step 2: Generate Candidate Events**

4: Generate inter-arrival times $\Delta t \sim \text{Exp}(\lambda_{\text{max}}^{(k)})$

5: Initialize $t_{\text{cand}} \leftarrow T_{\text{orig}}$

6: Initialize $i \leftarrow 1$

7: **while** $t_{\text{cand}} < T_{\text{end}}$ **do**

8: $\Delta t_i \sim \text{Exp}(\lambda_{\text{max}}^{(k)})$

9: $t_{\text{cand}}^{(i)} \leftarrow t_{\text{cand}} + \Delta t_i$

10: **Step 3: Accept/Reject Candidate Events**

11: Acceptance probability $p_{\text{accept}}^{(k)}\left(t_{\text{cand}}^{(i)}\right) = \frac{\lambda_k\left(t_{\text{cand}}^{(i)}\right)}{\lambda_{\text{max}}^{(k)}}$

12: Generate a uniform random number $u \sim \mathcal{U}(0, 1)$

13: **if** $u \leq p_{\text{accept}}^{(k)}\left(t_{\text{cand}}^{(i)}\right)$ **then**

14: Accept candidate event: $t_{\text{pad}}^{(i)} \leftarrow t_{\text{cand}}^{(i)}$

15: $i \leftarrow i + 1$

16: **end if**

17: $t_{\text{cand}} \leftarrow t_{\text{cand}}^{(i)}$

18: **end while**

19: **Step 4: Construct the Padding Event Sequence**

20: $\mathcal{T}_{\text{pad}}^{(k)} = \{t_{\text{pad}}^{(1)}, t_{\text{pad}}^{(2)}, \dots, t_{\text{pad}}^{(N_k)}\}$, where N_k is the number of accepted events

21: **if** number of generated events exceeds $T_{\text{pad}} = T_{\text{target}} - T_{\text{orig}}$ **then**

22: Use only the first T_{pad} events

23: **end if**

24: **return** $\mathcal{T}_{\text{pad}}^{(k)}$

C.5 The Immigration-Birth View and Stationarity

The immigration-birth representation provides an intuitive way to understand the Hawkes process as a Poisson cluster process.

- **Immigration Process:** A homogeneous Poisson process with rate λ . Events in this process represent exogenous shocks or external events that trigger the Hawkes process.
- **Birth Process:** Each immigration event occurring at time s generates a new inhomogeneous Poisson process (also known as a Poisson point process) with intensity $\mu(t - s)$ for

$t > s$. These events represent offspring or triggered events caused by the initial immigration event.

- **Hawkes Process:** The Hawkes process is the superposition of the immigration process and all the birth processes.

This representation allows us to analyze the Hawkes process using tools from branching process theory.

Definition C.15 (Branching Ratio). An event occurring at time s will generate a Poisson-distributed number of first-generation offspring over the time interval $[s, \infty)$. The expected number of offspring, known as the branching ratio, is defined as:

$$\eta = \int_s^\infty \mu(t-s) dt = \int_0^\infty \mu(t) dt. \quad (15)$$

THEOREM C.16 (STATIONARITY CONDITION). *The Hawkes process is stationary (i.e., the process does not explode) and has a finite mean if and only if the branching ratio is less than one:*

$$\eta < 1 \quad (16)$$

This condition ensures that, on average, each event generates less than one offspring, preventing the process from growing unbounded.

Example C.17 (Stationarity). If $\mu(t) = \alpha e^{-\beta t}$, then the branching ratio is:

$$\eta = \int_0^\infty \alpha e^{-\beta t} dt = \frac{\alpha}{\beta}. \quad (17)$$

Therefore, the process is stationary if and only if $\alpha < \beta$.

THEOREM C.18 (LAW OF LARGE NUMBERS). *Under the stationarity condition ($\eta < 1$), the long-term average rate of events converges to:*

$$\lim_{t \rightarrow \infty} \frac{N_t}{t} = \frac{\lambda}{1-\eta} \quad \text{a.s.} \quad (18)$$

This result provides an explicit formula for the long-run average rate in terms of the background rate and branching ratio.

C.6 Excitation Functions and Markov Analysis

The choice of excitation function $\mu(t)$ is critical for modeling specific characteristics of the self-exciting process.

- **Delayed Impact:** The excitation function can be designed to incorporate a delayed impact, where the influence of an event is not immediate but increases over time. This can be achieved using functions such as the gamma distribution pdf for $\mu(t)$.
- **Domain-Specific Expertise:** The excitation function can be tailored to incorporate domain knowledge. The Omori-Utsu law in seismology is an example of a power-law kernel used to model aftershock rates.

Definition C.19 (Omori-Utsu Law). The Omori-Utsu law models the aftershock rate following an earthquake:

$$\mu(t) = \frac{K}{(t+c)^p}, \quad (19)$$

where $K, c > 0$ and $p > 1$. The parameters control the magnitude, shift, and decay rate of the aftershock sequence.

The exponentially decaying excitation function $\mu(t) = \alpha e^{-\beta t}$ is particularly important due to the Markov property.

THEOREM C.20 (MARKOV PROPERTY). *When the excitation function is exponentially decaying, the joint process (N_t, λ_t^*) is a Markov process. This simplifies inference, simulation, and analysis because the future state of the process depends only on the current state and not on the entire past history.*

In particular, the conditional intensity between jumps $(T_n \leq t < T_{n+1})$ follows:

$$\lambda_t^* = \lambda + (\lambda_{T_n^*}^* - \lambda)e^{-\beta(t-T_n)} = \lambda + (\lambda_{T_n}^* + \alpha - \lambda)e^{-\beta(t-T_n)}. \quad (20)$$

Definition C.21 (Exponentially Decaying Hawkes Process). An exponentially decaying Hawkes process can be further generalized by allowing the conditional intensity to start at an initial value λ_0 that differs from the background rate λ . The conditional intensity for $t \geq 0$ is given by

$$\lambda_t^* = \lambda + (\lambda_0 - \lambda)e^{-\beta t} + \sum_{T_i < t} \alpha e^{-\beta(t-T_i)}. \quad (21)$$

The compensator for this process is:

$$\Lambda_t = \lambda t + \frac{(\lambda_0 - \lambda)}{\beta} (1 - e^{-\beta t}) + \sum_{T_i < t} \frac{\alpha}{\beta} (1 - e^{-\beta(t-T_i)}). \quad (22)$$

C.7 Likelihood-Based Inference

Maximum likelihood estimation (MLE) is a standard method for parameter estimation in Hawkes processes.

THEOREM C.22 (LIKELIHOOD FUNCTION FOR POINT PROCESSES). *The likelihood function for a point process with parameter vector θ , given observations $\{t_1, \dots, t_n\}$ within a time horizon $[0, T]$, is:*

$$\begin{aligned} L(\theta \mid t_1, \dots, t_n, T) &= \left[\prod_{i=1}^n \lambda_{t_i}^* \right] \exp\left(-\int_0^T \lambda_t^* dt\right) \\ &= \left[\prod_{i=1}^n \lambda_{t_i}^* \right] e^{-\Lambda_T}. \end{aligned} \quad (23)$$

THEOREM C.23 (LOG-LIKELIHOOD FUNCTION). *The corresponding log-likelihood function is:*

$$\ell(\theta \mid t_1, \dots, t_n, T) = \sum_{i=1}^n \log \lambda_{t_i}^* - \Lambda_T. \quad (24)$$

THEOREM C.24 (LOG-LIKELIHOOD FOR HAWKES PROCESS). *Substituting the Hawkes process conditional intensity, the log-likelihood function becomes:*

$$\ell(\theta \mid t_1, \dots, t_n, T) = \sum_{i=1}^n \log \left(\lambda + \sum_{t_j < t_i} \mu(t_i - t_j) \right) - \Lambda_T. \quad (25)$$

Direct numerical maximization of the log-likelihood is a common approach for parameter estimation. However, it may encounter convergence issues if the log-likelihood function is flat near its maximum.

C.8 In-Depth Discussion of the Intensity Function

The intensity function defined in Equation (1) is a sophisticated model designed to capture the complex dynamics of event sequences in micro-videos, particularly the cross-influence between

different types of events. Let’s dissect the function to understand its key components and motivations:

C.8.1 Core Motivation: Modeling Interdependent Event Sequences. The primary motivation behind this particular formulation stems from the observation that events in social media, such as likes, shares, comments, and favorites, are not independent. The occurrence of one type of event can significantly influence the probability of subsequent events of the same type (self-excitation) or different types (cross-excitation). Capturing these interdependencies is crucial for accurate modeling and prediction.

C.8.2 Deconstructing the Components. Let’s examine each term of the intensity function in detail:

- **Baseline Intensity (μ_k):** The term μ_k represents the intrinsic or baseline rate at which events of type k occur, independent of any past events. It accounts for factors such as the inherent appeal of the video or general user activity. This is a constant term, and guarantees that the conditional intensity is always positive.
- **Cross-Excitation Term ($\sum_{m=1}^4 \sum_{h: t_h^{(m)} < t} \alpha_{k,m} \exp(-\delta_{k,m}(t-t_h^{(m)}))$):** This is the heart of the model’s ability to represent cross-excitation.
 - **Inner Sum ($\sum_{h: t_h^{(m)} < t}$):** This sum iterates through all historical events of type m that occurred before time t . Each historical event contributes to the current intensity of event type k .
 - **Cross-Excitation Coefficient ($\alpha_{k,m}$):** The coefficient $\alpha_{k,m}$ is crucial. It quantifies the degree to which an event of type m influences the occurrence of events of type k .
 - * If $\alpha_{k,m} > 0$, it indicates that an event of type m *excites* (promotes or increases the likelihood of) events of type k . For example, a high number of likes ($m = \text{likes}$) might encourage more shares ($k = \text{shares}$).
 - * If $\alpha_{k,m} < 0$, it suggests that an event of type m *inhibits* (decreases the likelihood of) events of type k . This could happen in some scenarios; e.g., a large number of comments (which may include negative feedback) might discourage further likes. Although, in this function, it’s assumed that $\alpha_{k,m} > 0$.
 - * If $\alpha_{k,m} \approx 0$, it means that events of type m have little to no direct influence on events of type k .
 - * The magnitude of $\alpha_{k,m}$ reflects the strength of the influence. Larger absolute values imply stronger effects.
 - **Exponential Decay Function ($\exp(-\delta_{k,m}(t-t_h^{(m)}))$):** This function models the decaying influence of past events over time. The parameter $\delta_{k,m}$ determines the rate of decay.
 - * A larger $\delta_{k,m}$ implies a faster decay rate. The influence of the past event quickly diminishes.
 - * A smaller $\delta_{k,m}$ indicates a slower decay rate. The influence of the past event persists for a longer duration.
 - * The exponential form is chosen because it’s a simple, mathematically tractable way to represent this decaying influence. It captures the idea that recent events have a stronger impact than distant events.

- **Neural Network Term ($f_k(h(t))$):** This term introduces a non-linear component, capturing more complex dependencies and hidden factors that cannot be adequately modeled by the linear superposition of past event influences. This is typically used to inject features of the video into the conditional intensity calculation. The $h(t)$ represents some hidden state or representation learned by a neural network (Mamba in this specific instance) up to time t .

C.8.3 Advantages of this Formulation.

- **Flexibility:** This intensity function offers considerable flexibility in capturing a wide range of dependencies between different types of events.
- **Interpretability:** The parameters ($\mu_k, \alpha_{k,m}, \delta_{k,m}$) have clear interpretations, providing insights into the underlying dynamics of the event sequences.
- **Adaptability:** The integration of the neural network term allows the model to learn and adapt to complex, nonlinear patterns in the data.

C.8.4 Key Assumption: Additivity. A core assumption of this formulation is that the influences of past events are additive (through the summation). While this simplifies the model, it might not always be perfectly realistic. In some scenarios, event influences might interact in more complex, non-additive ways.

C.8.5 In Summary: A Holistic Model. This intensity function presents a holistic approach to modeling event sequences by: (1) establishing a basic arrival rate, (2) capturing the effect of past events from various sources that influence the present behavior, and (3) Incorporating intricate, high-order dependencies that may be discovered directly from data. Overall, it integrates interpretability with a more nuanced nonlinear component, providing a practical approach for event modeling.

C.9 Derivation and Rationale for the MHP Intensity Function

The formulation of the Mamba-Hawkes Process (MHP) intensity function, presented in Equation (1), represents a principled synthesis of the classical Hawkes process (Appendix C) and the Mamba state-space model (Appendix B). This section provides a detailed derivation to elucidate the connection between these components, justifying our model’s architecture.

A classical multivariate Hawkes process, as detailed in Appendix C.3, models the event intensity as a linear superposition of a baseline rate and contributions from past events, typically via an exponential decay kernel. This formulation, while interpretable, is predicated on the strong assumption that the influence of historical events is both additive and context-agnostic. That is, the impact of an event is predetermined by its type and time of occurrence, irrespective of the broader sequence of interactions in which it is embedded. This assumption is often violated in real-world scenarios like micro-video engagement, where the dynamics are highly non-linear. For instance, an initial surge of likes might be positively reinforcing, but their influence could be completely negated or even reversed by a subsequent wave of negative comments. A classical Hawkes model is structurally incapable of capturing such complex, context-dependent modulations of influence.

To address this fundamental limitation, we augment the classical Hawkes formulation with a dynamic, non-linear component derived from a Mamba model. As described in Appendix B, Mamba is a selective state-space model adept at capturing long-range dependencies in sequential data. When applied to a sequence of user interactions $\mathcal{R} = \{(t_0, y_0), \dots, (t_n, y_n)\}$, the Mamba module processes the entire event history and distills it into a compressed, history-aware hidden state vector, $h(t)$. This vector is not a mere aggregation but a rich representation that encodes the intricate sequential and causal dependencies among past events.

The bridge between the two paradigms is the function $f_k(h(t))$ in our MHP intensity function. We posit that the full intensity of an event is determined not only by the linear excitation from past events but also by a non-linear correction based on the global context of the event history. The Mamba-generated state $h(t)$ provides this global context. The term $f_k(h(t))$, which is implemented as a small neural network that takes $h(t)$ as input, serves as this dynamic correction factor. It can output positive or negative values, allowing it to adaptively increase or decrease the event intensity. For example, if $h(t)$ represents a history of waning engagement, $f_k(h(t))$ can output a negative value that suppresses the intensity calculated by the classical Hawkes components, thereby accurately modeling a ‘‘Later Decline’’ phase.

Thus, the complete MHP intensity function from Equation (1),

$$\lambda_k(t) = \mu_k + \sum_{m=1}^M \sum_{t_i^{(m)} < t} \alpha_{k,m} e^{-\delta_{k,m}(t-t_i^{(m)})} + f_k(h(t)),$$

is a composite model. It retains the interpretable baseline intensity (μ_k) and the linear, exponentially decaying influence from past events (the summation term) of the classical Hawkes process. Crucially, it enhances this foundation with the term $f_k(h(t))$, which leverages the powerful sequence modeling capabilities of Mamba to introduce a non-linear, context-aware correction. This synergistic integration allows the MHP to capture the nuanced, dynamic, and often non-monotonic trajectories of micro-video popularity far more faithfully than either of its constituent models could alone.

D Justification for Using Ogata’s Thinning Algorithm for Temporal Embeddings

In this section, we provide a detailed justification for our choice to employ Ogata’s thinning algorithm to generate fixed-length temporal embeddings from the Mamba-Hawkes Process (MHP). This design choice was rightly questioned, noting that modern architectures like Mamba can inherently process variable-length sequences. Our rationale is rooted in the specific requirements of the downstream **temporal-aware retrieval module** and our objective to maintain the highest possible fidelity in the temporal representation while enabling efficient, large-scale similarity search.

D.1 The Core Challenge: Efficient and Meaningful Similarity Search

The primary goal of our retrieval module is to identify historical videos that are similar to a target video along two axes: multi-modal content and *temporal popularity dynamics*. For a retrieval system to be practical, especially when querying a large memory bank (B)

containing millions of candidates, the similarity computation must be highly efficient. The dot product, as used in our temporal similarity calculation ‘‘SStemp’’ (Equation 3), is one of the most efficient methods for comparing two vector representations. It forms the backbone of modern large-scale vector search systems (e.g., FAISS, ScaNN). This operation, however, fundamentally requires that the two vectors being compared have a fixed, identical dimensionality.

This requirement presents a direct conflict: our Mamba-Hawkes Process (MHP) naturally produces a variable-length sequence of hidden states corresponding to the variable number of user interaction events, but our retrieval mechanism is most efficient with fixed-length vectors. The crucial question then becomes: how do we best transform a variable-length, event-driven temporal representation into a fixed-length vector with minimal loss of information?

D.2 Limitations of Naive Alternatives (e.g., Pooling)

A common approach to creating a fixed-size representation from a variable-length sequence is to use a pooling operation (e.g., mean-pooling or max-pooling) on the sequence of MHP outputs. We argue that such an approach, while simple, is fundamentally inadequate for our task and would undermine the very motivation for using a sophisticated temporal model like the MHP.

- **Mean-Pooling:** Applying mean-pooling would average the temporal dynamics over the entire event sequence. This would effectively smooth out and destroy the precise ‘‘rollercoaster-like’’ patterns—the initial surges, the subsequent decays, the bursts of activity—that we aim to capture. A video with a sharp early peak and rapid decline would become indistinguishable from a video with slow, steady growth if their average event intensity is similar. This is a highly ‘‘lossy’’ compression that discards the most discriminative temporal information.
- **Max-Pooling:** Max-pooling would only capture the single most intense moment of user interaction, ignoring the overall shape, duration, and decay characteristics of the popularity curve. It cannot differentiate between a flash-in-the-pan viral event and one that builds to a peak and sustains interest.
- **Last Hidden State:** Using the last hidden state of the Mamba model is another common technique. While this encodes information from the entire sequence, its representation is heavily biased towards the most recent events, failing to provide a balanced summary of the overall temporal trajectory, especially the crucial early-stage dynamics.

In short, while these simpler alternatives would solve the fixed-length problem, they would do so by discarding the nuanced, sequential, and causal information that our MHP module is specifically designed to model.

D.3 Ogata’s Thinning as a Principled, High-Fidelity Solution

In contrast to the naive methods above, Ogata’s thinning algorithm [5] is not merely a ‘‘padding’’ technique. It is a **statistically principled simulation method**. Instead of adding meaningless

zero-vectors or applying a lossy pooling function, the thinning algorithm generates a new, longer event sequence that is a *statistically faithful realization* of the very same Non-Homogeneous Poisson Process (NHPP) learned by our MHP model.

The process works as follows:

- We first learn the complex, time-varying intensity function $\lambda_k(t)$ for a given video using our MHP module. This function represents the instantaneous probability of an event of type k occurring at any time t .
- We establish a constant upper bound, λ_{\max} , for this intensity function over the time interval of interest.
- We then generate candidate events from a simpler, homogeneous Poisson process with a constant rate λ_{\max} .
- Each candidate event at time t_{cand} is "thinned" (i.e., accepted or rejected) with a probability of $\lambda_k(t_{\text{cand}})/\lambda_{\max}$.

The resulting sequence of accepted events is guaranteed to be a valid sample from the original, complex NHPP defined by $\lambda_k(t)$. By running this simulation until we obtain a pre-defined number of events (our fixed length), we are effectively "completing" the popularity trajectory according to the learned dynamics.

D.4 Maintaining Fidelity and Creating a Canonical Representation

The key advantage of this approach is its **high fidelity**. The simulated events are not noise; they are plausible future events that *could have happened* according to the model’s understanding of the video’s temporal dynamics. This allows us to create what we term a **canonical temporal signature**. By simulating all interaction sequences to the same fixed length, we are standardizing them not based on their observed history (which can be sparse or short), but based on the underlying temporal process they represent.

This provides a much richer and more robust basis for comparison:

- A video with a high initial intensity will be simulated to have more events early in its canonical signature.
- A video with a slow decay rate will show a more sustained pattern of events throughout its signature.

This allows our dot-product similarity to directly compare the fundamental temporal *shapes* of popularity curves, which was our original goal.

D.5 Conclusion

In summary, the decision to use Ogata’s thinning algorithm was a deliberate engineering and modeling choice to resolve the tension between the need for a high-fidelity, variable-length temporal representation and the practical requirement for an efficient, fixed-length vector for large-scale retrieval. Simpler methods like pooling were considered and rejected due to their lossy nature, which would compromise the core contribution of our temporal modeling. The thinning algorithm provides a statistically sound method to generate a fixed-length canonical temporal signature, preserving the intricate dynamics captured by the MHP and enabling meaningful and efficient similarity calculations. We thank the reviewer for this insightful question, which has allowed us to clarify this critical

aspect of our methodology. This careful balance between representation fidelity and retrieval efficiency is a key contribution of our work.

E Multi-Modal Feature Extraction

For MVPP, it is fatal to extract the required feature information from the multi-modal information of the video. We perform frame-by-frame processing on all target videos, select certain interval frames for extracting image and audio information, and transform them into corresponding frame feature vectors through Vision Transformer (ViT) [9] and Audio Spectrogram Transformer (AST) architectures [14]. Further, we input the image-audio features of the video and the text description into a model with both forward and reverse attention mechanisms to capture its content features. Further, we compare it with the videos matched by the retriever in the database to further enhance this feature.

To capture the key features of a micro video V_i , we extract visual, audio and textual information. We start by selecting key frames $F_1^i, F_2^i, \dots, F_K^i$, where K is the total number of frames. Each frame $F_j^i \in \mathbb{R}^{H \times W \times C}$ is divided into fixed-size patches and reshaped $F_j^{i*} \in \mathbb{R}^{N_p \times P^2 \times C}$, where (H, W) is the resolution of the original frame, C is the number of channels, (P, P) is the patch size, and N_p is the number of patches, which serves as the input sequence length for the Vision Transformer (ViT) [9]. Through ViT, visual information of video frames is encoded into visual embedding $E_i^v \in \mathbb{R}^{K \times d_v}$, where d_v denotes the length of a single embedding.

For audio features, we follow a similar approach using the Audio Spectrogram Transformer (AST). We first align the timestamps of the sampled frames with corresponding audio segments $W = \{w_1, w_2, \dots, w_K\}$ extracted from the video’s soundtrack. These audio segments are processed using a Fast Fourier Transform (FFT) [34] to generate Mel-frequency spectral coefficients (MFCC), resulting in a spectrum matrix $M_S \in \mathbb{R}^{n_{mel} \times n_a}$, where n_{mel} is the number of mel-filters, and n_a is the number of time frames, determined by the audio length and stride. This spectrum matrix, treated as a single-channel image, is then processed using the same patching method applied to visual frames and transformed into acoustic embedding $E_i^a \in \mathbb{R}^{K \times d_a}$, where d_a denotes the length of a single embedding.

Next, these feature matrices are concatenated to emphasize the relationship between visual and audio information:

$$E_i^{v,a} = E_i^v \oplus E_i^a \in \mathbb{R}^{K \times (d_v + d_a)}. \quad (26)$$

The concatenated features $E_i^{v,a}$ are then passed through a linear layer $W_c \in \mathbb{R}^{(d_v + d_a) \times d}$ with a ReLU activation function, generating an audio-visual embedding X_i^c . Similarly, we can get $E_i^t \in \mathbb{R}^{n_w \times d_t}$ through a pre-trained sentence embedding model *AngIE*, where n_w is the word length in the textual descriptions and d_t denotes the length of an embedded token. And then we acquire the textual embedding X_i^t through a linear layer $W_t \in \mathbb{R}^{d_t \times d}$:

$$X_i^c = \text{ReLU}(E_i^{v,a} W_c) \in \mathbb{R}^{K \times d}, \quad (27)$$

$$X_i^t = \text{ReLU}(E_i^t W_t) \in \mathbb{R}^{n_w \times d}. \quad (28)$$

F Feature Fusion and Popularity Prediction

F.1 Cross-modal/temporal Attention

Aligning audio-visual, textual modalities and temporal series of micro videos presents challenges due to potential inconsistencies between these three kinds of features: textual descriptions, audio-visual content and user feedback time-series. To address this, we implement three pairs of cross-attention network across three modal/temporal. The cross modal-temporal attention comprises both positive and negative attention modules, designed to capture the similarities and differences between multi-modal/temporal information. The positive attention module focuses on identifying the most consistent features across different modalities, while the negative attention module highlights any inconsistent or contradictory information.

To illustrate, we initially examine the cross-attention mechanism between the audio-visual and textual modalities as a representative case.

Within the positive attention module, the most aligned features between modalities are calculated using cross-modal/temporal attention vectors. For a given video V_i , the audio-visually guided positive textual features $T_i^{\mathcal{P}}$ and the textually guided positive audio-visual features $C_i^{\mathcal{P}}$ are derived as follows:

$$\begin{aligned} T_i^{\mathcal{P}} &= ATT^{\mathcal{P}}(X_i^c W_{\mathcal{P}}^Q, X_i^t W_{\mathcal{P}}^K, X_i^t W_{\mathcal{P}}^V) \\ &= Softmax(\alpha \frac{QK^T}{\sqrt{d}}) \mathcal{V}, \end{aligned} \quad (29)$$

$$\begin{aligned} C_i^{\mathcal{P}} &= ATT^{\mathcal{P}}(X_i^t W_{\mathcal{P}}^Q, X_i^c W_{\mathcal{P}}^K, X_i^c W_{\mathcal{P}}^V) \\ &= Softmax(\alpha \frac{QK^T}{\sqrt{d}}) \mathcal{V}, \end{aligned} \quad (30)$$

where ATT function represents the Attention mechanism, α is the positive scaling factor, X_i^c denotes the embedding generated from audio-visual extraction and X_i^t is the input of textual embedding. Besides, $W_{\mathcal{P}}^Q, W_{\mathcal{P}}^K, W_{\mathcal{P}}^V$ denote the query, key, and value projection matrices, respectively. The parameter α is used to balance the influence of positive and negative attention. Similarly, the negative audio-visually guided textual features $T_i^{\mathcal{N}}$ and textual guided audio-visual features $C_i^{\mathcal{N}}$ can be obtained as follows, where $\gamma = -(1 - \alpha)$ is the negative scaling factor:

$$\begin{aligned} T_i^{\mathcal{N}} &= ATT^{\mathcal{N}}(X_i^c W_{\mathcal{N}}^Q, X_i^t W_{\mathcal{N}}^K, X_i^t W_{\mathcal{N}}^V) \\ &= Softmax(\gamma \frac{QK^T}{\sqrt{d}}) \mathcal{V}, \end{aligned} \quad (31)$$

$$\begin{aligned} C_i^{\mathcal{N}} &= ATT^{\mathcal{N}}(X_i^t W_{\mathcal{N}}^Q, X_i^c W_{\mathcal{N}}^K, X_i^c W_{\mathcal{N}}^V) \\ &= Softmax(\gamma \frac{QK^T}{\sqrt{d}}) \mathcal{V}. \end{aligned} \quad (32)$$

After this, we referred to the integration processing of hidden states in the MMRA [11] [45] model to generate a comprehensive textual modal representation in FFN layers, incorporate audio-visual hidden states into textual hidden states to generate a comprehensive textual, audio-visual modal representation \tilde{T}_i and \tilde{C}_i ,

which modify the calculation of the FFN process as follows:

$$\tilde{T}_i^c = ReLU \left(X_i^t + \left(C_i^{\mathcal{P}} \oplus C_i^{\mathcal{N}} \right) W_1^t \right) W_2^t, \quad (33)$$

$$\tilde{C}_i^c = ReLU \left(X_i^c + \left(T_i^{\mathcal{P}} \oplus T_i^{\mathcal{N}} \right) W_1^c \right) W_2^c, \quad (34)$$

where $W_1^t, W_1^c \in \mathbb{R}^{2d \times d}, W_2^t, W_2^c \in \mathbb{R}^{d \times d}$ represent learnable weights matrix via the attentive pooling strategy, \oplus denotes the concatenation operation.

Similarly, T_i^s, S_i^t and C_i^s, S_i^t can be obtained through textual-temporal and audiovisual-temporal cross-attention respectively. Finally, we exploit expressive representations T_i, C_i, S_i by concatenation and transformation, followed by the attentive pooling strategy [37].

F.2 Retrieval Enhanced Interaction and Prediction

We focus on extracting valuable insights from relevant videos retrieved to improve micro video popularity prediction (MVPP). The retrieved videos hold the similar multi-modal/temporal patterns with the target video, which enhance the characteristic of the target video.

The retrieved feature from Multi-modal/temporal Retrieval (see section 4.3) can be integrated into the cross-attention structure and effectively learned. We employ the same process on the retrieved embeddings $X_i^{r,c}, X_i^{r,t}$ and $X_i^{r,t}$, to calculate T_i^r, C_i^r and S_i^r . For information augmentation, we also encode the retrieved label embedding L_i^r of each video V_i . Finally, we integrate all features from the micro-video $V_i: T_i, C_i, S_i$ and T_i^r, C_i^r, S_i^r , along with the retrieved labels L_i^r . Thus, we could construct cross-sample interactions as follows:

$$I = [\Phi(C_i, C_i^r), \Phi(C_i, T_i^r), \Phi(C_i, S_i^r), \dots, \Phi(S_i, S_i^r), \Phi(S_i, L_i^r)],$$

where Φ denotes the process of inner products.

In the end, we put all the components into a prediction network. For the micro-video V_i , the output layer is fed with the concatenated vector as $H = concat([T_i, C_i, S_i, T_i^r, C_i^r, S_i^r, L_i^r, I])$. The output layer is multilayer perceptrons (MLPs) with one final output unit to predict the popularity (heart, share, play, comment) of the target video.

G Assumptions and Proof Sketch for Theorem 1

The oracle properties of the MHP estimator, as stated in Theorem 3.2.3, hold under the following standard assumptions.

Assumption 1 (Stationarity and Ergodicity). The true Hawkes process $N(t; \theta^*)$ is stationary and ergodic. This requires the spectral radius of its branching ratio matrix to be less than 1. This ensures that the Law of Large Numbers and Central Limit Theorem apply to the log-likelihood and its derivatives.

Assumption 2 (Model Identifiability). The parameterization is identifiable. If $\theta_1 \neq \theta_2$, then the corresponding probability laws of the Hawkes processes differ.

Assumption 3 (Regularity Conditions). The log-likelihood function $\ell(\theta)$ is twice continuously differentiable with respect to θ in a neighborhood of θ^* . The Fisher information matrix $I(\theta) = -E[\nabla^2 \ell(\theta)]$ is finite and positive definite at $\theta = \theta^*$.

Assumption 4 (Penalty Function). The penalty function $p_{\gamma_N}(t)$ is a non-decreasing and concave function for $t > 0$. Its derivative

$p'_{\gamma_N}(t)$ must satisfy that for some $a > 1$, $p'_{\gamma_N}(t) = \gamma_N$ for $t \approx 0^+$ and $\lim_{t \rightarrow \infty} p'_{\gamma_N}(t) = 0$. The regularization parameter is chosen such that as $N \rightarrow \infty$, $\gamma_N \rightarrow 0$ and $\sqrt{N}\gamma_N \rightarrow \infty$. This is satisfied by the MCP and SCAD penalties.

The proof proceeds by analyzing the Karush-Kuhn-Tucker (KKT) conditions for the penalized likelihood estimator $\hat{\theta}_N$, showing that with probability approaching 1, any solution satisfying these conditions exhibits the desired oracle properties: sparsity recovery and asymptotic normality equivalent to the oracle estimator.

Under Assumptions 1–3, it follows from the theory of M-estimators for point processes that there exists a \sqrt{N} -consistent local maximizer $\hat{\theta}_N$ of the penalized likelihood function, satisfying $\|\hat{\theta}_N - \theta^*\| = O_p(N^{-1/2})$. This consistency allows the analysis to be localized to a shrinking neighborhood of the true parameter θ^* .

A necessary condition for $\hat{\theta}_N$ to be a local maximizer is that the subgradient of the objective function contains zero, yielding the KKT conditions for $j = 1, \dots, p$:

$$\frac{\partial L_N(\hat{\theta}_N)}{\partial \theta_j} - p'_{\gamma_N}(|\hat{\theta}_{N,j}|) \text{sign}(\hat{\theta}_{N,j}) = 0 \quad \text{if } \hat{\theta}_{N,j} \neq 0, \quad (35)$$

$$\left| \frac{\partial L_N(\hat{\theta}_N)}{\partial \theta_j} \right| \leq p'_{\gamma_N}(0) \quad \text{if } \hat{\theta}_{N,j} = 0. \quad (36)$$

By Assumption 4, $p'_{\gamma_N}(0) = \gamma_N$. The analysis is divided into the true non-zero coefficients (indexed by \mathcal{A}) and the true zero coefficients (indexed by \mathcal{A}^c).

To establish sparsity recovery, we show that $\hat{\theta}_{N,j} = 0$ for all $j \in \mathcal{A}^c$ with probability approaching 1. Consider a candidate solution of the form $\hat{\theta} = (\hat{\theta}_{\mathcal{A}}, \mathbf{0}_{\mathcal{A}^c})$. For this to satisfy the KKT conditions, it must hold that $|\partial L_N(\hat{\theta})/\partial \theta_j| \leq \gamma_N$ for each $j \in \mathcal{A}^c$.

A Taylor expansion of $\partial L_N(\hat{\theta})/\partial \theta_j$ around θ^* gives

$$\frac{\partial L_N(\hat{\theta})}{\partial \theta_j} = \frac{\partial L_N(\theta^*)}{\partial \theta_j} + \nabla_{\theta_j}^2 L_N(\theta^*)(\hat{\theta} - \theta^*) + o_p(N^{-1/2}). \quad (37)$$

The score term $\partial L_N(\theta^*)/\partial \theta_j$ is $O_p(N^{-1/2})$ by the central limit theorem for martingales, while the Hessian term is also $O_p(N^{-1/2})$ due to the consistency of $\hat{\theta}$ and the convergence of $\nabla^2 L_N(\theta^*)$ to the finite Fisher information matrix. Thus, $|\partial L_N(\hat{\theta})/\partial \theta_j| = O_p(N^{-1/2})$ for $j \in \mathcal{A}^c$.

The condition $O_p(N^{-1/2}) \leq \gamma_N$ holds with probability approaching 1, as Assumption 4 implies $\sqrt{N}\gamma_N \rightarrow \infty$, so γ_N decays slower than $N^{-1/2}$. Therefore, the KKT conditions are satisfied with $\hat{\theta}_{N,j} = 0$ for all $j \in \mathcal{A}^c$ with probability tending to 1, establishing sparsity recovery.

For the asymptotic normality of the active set, note that $\hat{\theta}_{N,\mathcal{A}}$ is consistent for $\theta_{\mathcal{A}}^*$ and $\gamma_N \rightarrow 0$. Thus, for sufficiently large N , $\min_{j \in \mathcal{A}} |\theta_j^*| > a\gamma_N$, and by consistency, $|\hat{\theta}_{N,j}| > a\gamma_N$ for $j \in \mathcal{A}$ with probability approaching 1. By the SCAD-type penalty property in Assumption 4, this implies $p'_{\gamma_N}(|\hat{\theta}_{N,j}|) = 0$ for $j \in \mathcal{A}$.

The KKT conditions for \mathcal{A} then reduce to

$$\frac{\partial L_N(\hat{\theta}_{N,\mathcal{A}}, \mathbf{0}_{\mathcal{A}^c})}{\partial \theta_j} = 0, \quad j \in \mathcal{A}, \quad (38)$$

which matches the score equations for the oracle maximum likelihood estimator assuming knowledge of \mathcal{A} .

A first-order Taylor expansion around $\theta_{\mathcal{A}}^*$ yields

$$\mathbf{0} \approx \nabla_{\theta_{\mathcal{A}}} L_N(\theta^*) + \nabla_{\theta_{\mathcal{A}}}^2 L_N(\theta^*)(\hat{\theta}_{N,\mathcal{A}} - \theta_{\mathcal{A}}^*). \quad (39)$$

Rearranging and scaling by \sqrt{N} gives

$$\sqrt{N}(\hat{\theta}_{N,\mathcal{A}} - \theta_{\mathcal{A}}^*) \approx -(\nabla_{\theta_{\mathcal{A}}}^2 L_N(\theta^*))^{-1} \sqrt{N} \nabla_{\theta_{\mathcal{A}}} L_N(\theta^*). \quad (40)$$

By the law of large numbers for ergodic processes, $-\nabla_{\theta_{\mathcal{A}}}^2 L_N(\theta^*) \xrightarrow{P} \mathbf{I}_{\mathcal{A},\mathcal{A}}(\theta^*)$. By the central limit theorem for martingales,

$$\sqrt{N} \nabla_{\theta_{\mathcal{A}}} L_N(\theta^*) = \frac{1}{\sqrt{N}} \sum_{i=1}^N \nabla_{\theta_{\mathcal{A}}} \ell_i(\theta^*) \xrightarrow{d} \mathcal{N}(0, \mathbf{I}_{\mathcal{A},\mathcal{A}}(\theta^*)). \quad (41)$$

Applying Slutsky's theorem, we obtain

$$\sqrt{N}(\hat{\theta}_{N,\mathcal{A}} - \theta_{\mathcal{A}}^*) \xrightarrow{d} \mathcal{N}(0, \mathbf{I}_{\mathcal{A},\mathcal{A}}^{-1}(\theta^*)), \quad (42)$$

establishing asymptotic normality and the oracle property.

H Analysis of Computational Complexity and Deployment Feasibility

A valid concern regarding our M³TR framework is its apparent complexity, given the integration of multiple large pre-trained models and sophisticated custom modules. In this section, we provide a transparent and detailed analysis of the computational costs and argue for the framework's practical feasibility and scalability in a real-world, large-scale micro-video recommendation environment.

Our framework's architecture is predicated on a crucial design principle: **decoupling the expensive, large-scale data processing from the low-latency, real-time prediction task**. This is achieved through a two-phase process: (1) Offline Memory Bank Construction and (2) Online Real-time Inference.

H.1 Phase 1: Offline Memory Bank Construction

This phase involves pre-processing every video in the historical corpus to build the comprehensive Memory Bank (B). This is a one-time, upfront cost per video. The key operations are:

- **Multi-Modal Feature Extraction:** For each video, we extract visual (ViT), acoustic (AST), and textual (Angle) embeddings. Using a cluster of GPUs, a corpus of millions of videos can be processed in batches with high throughput. The amortized cost per video is constant.
- **Temporal Embedding Generation:** This involves training the Mamba-Hawkes Process (MHP) on user interaction sequences and then using it to generate the temporal embedding X_i^t . MHP training is the most novel and intensive part of this offline stage, but once trained, inference to produce the embeddings is fast. This step is also fully parallelizable across all videos.
- **Unified Retrieval Vector Generation:** We use powerful but heavy models like BLIP-2 and CLAP to generate rich textual descriptions from visual and audio content, which are then encoded into a unified semantic vector R_i . This is computationally expensive but, again, a one-time offline cost that can be distributed across multiple machines.

Practicality: This offline batch-processing paradigm is standard industry practice for large-scale systems at companies like Google/YouTube, Meta, and ByteDance. The computational budget for offline data preparation is significant but considers a necessary investment to enable high-quality online services. Our approach fits perfectly within this established operational model.

To provide a concrete cost estimate, processing the MicroLens-100k training set (approx. 15,779 videos) on our experimental setup of 16 NVIDIA A100 GPUs has the following approximate wall-clock times:

- Multi-Modal and Unified Vector Extraction (the most intensive part) requires approximately 12 hours of computation across the cluster.
- MHP inference, after a one-time training phase of ~8 hours, is significantly faster, taking less than 2 hours for the entire set.

The total amortized cost is manageable and aligns with typical data-pre-processing pipelines in industry.

H.2 Phase 2: Online Real-time Inference

This is the latency-critical phase, which occurs when a new target video arrives for popularity prediction. The process is designed to be extremely lightweight:

- **Feature Extraction (for Target Video):** The same feature extraction process from Phase 1 is applied to the single incoming video. On modern GPU hardware, processing a short micro-video through models like ViT and AST takes on the order of milliseconds.
- **Temporal-Aware Retrieval:** This step is the core of our system’s efficiency. A naive search through millions of vectors in the Memory Bank would be prohibitively slow ($O(N)$, where N is the bank size). Instead, we leverage state-of-the-art **Approximate Nearest Neighbor (ANN)** search algorithms and libraries, such as FAISS [22] or ScaNN [16]. These systems use techniques like quantization and graph-based indexing to perform the retrieval in sub-linear, typically logarithmic, time ($O(\log N)$). For a bank of millions or even billions of videos, an ANN lookup takes only a few milliseconds.
- **Retrieval-Enhanced Fusion and Prediction:** After retrieving the top- S exemplars (where S is a small, fixed hyperparameter, e.g., $S = 10$), the final prediction is made. The computational cost of this step is dominated by the cross-attention mechanisms between the target video’s features and the S retrieved feature sets. The complexity is roughly $O(S \cdot d^2)$, where d is the embedding dimension. Since both S and d are small constants, this cost is low, fixed, and, critically, *independent of the total size of the Memory Bank*.

H.3 Addressing Pipeline Brittleness

We acknowledge that maintaining a complex pipeline requires robust engineering practices. In a production environment, our framework would be implemented with the following considerations to ensure stability and robustness:

- **Model Versioning:** Each component (e.g., ViT or BLIP-2) would be versioned. Updates to any single model would trigger the creation of a new, versioned Memory Bank, allowing for safe A/B testing without disrupting the live system.
- **Monitoring and Alerting:** Each stage of the pipeline would be monitored for data drift, concept drift, and performance degradation. For instance, we would track the distribution of output embeddings and the ANN retrieval latency.
- **Fallback Strategies:** In case of a failure in a complex component (e.g., the MHP module), the system can be designed to gracefully degrade. For example, it could fall back to a simpler retrieval mechanism that relies only on content similarity (SS_modal), ensuring service availability.

H.4 Our Framework’s Superiority and Justification for Complexity

The analysis in Table 3 highlights the superiority of our design. We strategically accept a higher offline computational budget to achieve two critical goals for a real-world system:

- **State-of-the-Art Accuracy:** As our experimental results demonstrate (e.g., up to 19.3% nMSE improvement), the rich features generated by the “heavy” offline models and the novel MHP module provide a significant lift in prediction accuracy over simpler methods. This level of performance is often a key business differentiator.
- **Low-Latency Online Performance:** By pre-computing all expensive representations and leveraging efficient ANN indexing, our online inference latency remains low and constant, making it fully suitable for user-facing applications where predictions are needed in real-time.

In conclusion, the complexity of M³TR is not a liability but a deliberate and justified trade-off. It mirrors the engineering reality of modern large-scale recommendation systems, where offline processing power is leveraged to its fullest to provide fast, intelligent, and accurate online services. The framework is not only deployable but is architected in a way that is highly scalable and practical for the very environments it is designed to enhance.

I Baseline Models

- **SVR:** Uses Gaussian kernel-based Support Vector Regression (SVR) to predict micro-video popularity.
- **HyFea:** Employs the CatBoost tree model, leveraging multiple features (image, category, space-time, user profile, tags) for accurate prediction.
- **Contextual-LSTM:** Integrates contextual features into the LSTM model, capturing long-range context to improve prediction accuracy.
- **TMALL:** Introduces a common space to handle modality relatedness and limitations, enhancing popularity prediction.
- **MASSL:** Utilizes a multi-modal variational auto-encoder model, capturing cross-modal correlations to predict popularity.
- **MTFM:** Combines fuzzy trend matching and Informer in a multi-step prediction model, forecasting popularity trends.

Component	Computational Cost	Phase	Notes on Scalability
Memory Bank Construction			
Multi-Modal Extraction (ViT, AST)	High (per video)	Offline	Embarrassingly parallel; scales with GPU cluster size.
MHP Temporal Embedding	Moderate (per video)	Offline	Fully parallelizable; amortized cost is low.
Unified Retrieval Vector (BLIP-2, CLAP)	Very High (per video)	Offline	One-time cost; standard practice for deep content understanding.
Real-time Inference			
Feature Extraction (Target Video)	Low	Online	Milliseconds on a single GPU.
ANN Retrieval (e.g., FAISS)	$O(\log N)$	Online	Highly scalable; sub-linear time complexity w.r.t. Memory Bank size N .
Fusion & Prediction (Cross-Attention)	$O(S \cdot d^2)$	Online	Low and constant; independent of N . Dominant factor is small S .

Table 3: Computational Analysis of M³TR Components.

- **HMMVED**: Extracts and fuses multi-modal features through a variational information bottleneck for better prediction.
- **CBAN**: Applies cross-modal bipolar attention mechanisms, effectively capturing correlations in multi-modal data to enhance prediction.
- **MMRA**: Enhances prediction by retrieving relevant instances from a multi-modal memory bank and augmenting the prediction process.

J Datasets Details

MicroLens-100 [32] is a large-scale micro-video recommendation dataset designed to address the challenge of the lack of publicly available large-scale datasets in the field of micro-video recommendation. The dataset contains approximately one billion user-item interaction records, 34 million users, and one million micro-videos. In addition to user interactions with micro-videos, MicroLens-100k includes various raw modalities of video information, such as titles, cover images, audio, and full-length videos.

As a content-driven benchmark for micro-video recommendation, MicroLens-100k enables researchers to leverage multiple modalities of video information for recommendation, rather than relying solely on item IDs or pre-trained network-extracted generic video features. This provides a reliable testing platform for the development of micro-video recommendation systems and fosters innovation and progress in the recommendation system field.

Besides, another dataset we used is provided by 2024 IN- FORMS Data Challenge committee. Detailed information is listed in Table 4.

Dataset	#Video	#User	#Train	#Val	#Test
MicroLens-100k	19,724*	100,000	15779	1973	1972
2024 INFORMS Challenge	2200	8625	1760	220	220

*: 14 videos are disposed due to file corruption.

Table 4: Statistics of dataset.

The existing datasets are listed in Table 5, most of which are outdated and fail to reflect current multimodal, high-frequency user interactions, thus unable to realistically simulate real-world scenarios or accurately test algorithm performance.

Dataset	Modality					Scale	
	Text	r-Image	Audio	Video	User-feedback	#User	#Item
Tenrec	×	×	×	×	×	6.41M	4.11M
Flickr	×	×	×	×	×	8K	105K
Pinterest	×	✓	×	×	×	46K	880K
WikiMedia	×	✓	×	×	×	1K	10K
Behance	×	×	×	×	×	63K	179K
KuaiRand	×	×	×	×	×	27K	32.03M
KuaiRec	×	×	×	×	×	7K	11K
Reasoner	✓	✓	×	×	×	3K	5K
MicroLens	✓	✓	✓	✓	✓	30M	1M
INFORMS	✓	✓	✓	✓	✓	~ 350	2.2K
TikTokActions	✓	×	✓	✓	×		283.5K
Kaggle TikTok Video	✓	×	×	✓	✓		
Vine Dataset	✓	×	×	✓	✓	98.2K	303.2K
News on TikTok	✓	×	✓	✓	×		>4K
Kaggle TikTokDataset	×	×	×	✓	×		>100K img
YouTube Trending Videos	✓	×	×	✓	✓		
Snapchat Spotlight	✓	×	×	✓	✓		90K
YouTube-8M	×	×	✓	✓	×		6.1M
Instagram Reels Dataset	✓	×	×	×	×		
HowTo100M	✓	×	×	×	×		>1.2M
WebVid	✓	×	✓	✓	×		2M-10M
HD-VILA	✓	×	×	✓	×		3.3M
MMSum	✓	×	✓	✓	×		5.1K
InternVid	✓	×	✓	✓	×		7M

Table 5: Dataset comparison. “r-Image” refers to images with raw image pixels. “Audio” and “Video” mean the original full-length audio and video content.

K Evaluation Metrics Details

The main evaluation metric $nMSE$ is defined as follows:

$$nMSE = \frac{1}{N\sigma_{y_i}^2} \sum_{i=1}^N (y_i - \hat{y}_i)^2, \quad (43)$$

where N represent the total number of micro-video samples, y_i and \hat{y}_i are the target and predicted popularity score for the i th micro-video sample, and σ_{y_i} is the standard deviation of the target popularity.

In addition, we measure Spearman’s Rank Correlation (SRC) coefficient, Pearson linear correlation coefficient (PLCC), and Mean Absolute Error (MAE) as complementary metrics. SRC, PLCC, and MAE are defined as follows:

$$SRC = 1 - \frac{6 \sum d_i^2}{N(N^2 - 1)}, \quad (44)$$

$$MAE = \frac{1}{N} \sum_{i=1}^N |y_i - \hat{y}_i|, \quad (45)$$

$$PLCC = \frac{1}{N} \sum_{i=1}^N \frac{1}{T} \sum_{j=1}^T \left(\frac{y_i^j - \bar{y}_i}{\sigma_{y_i}} \right) \left(\frac{\hat{y}_i^j - \bar{\hat{y}}_i}{\sigma_{\hat{y}_i}} \right), \quad (46)$$

where d_i is the rank difference of a micro-video between the prediction and the popularity target. σ_{y_i} and $\sigma_{\hat{y}_i}$ stand for the standard deviation of the target and predicted popularity sequences for the i -th micro-video sample.

A higher SRC value indicates a stronger monotonic correlation between targets and predictions, a higher PLCC value indicates a higher model performance, while a lower nMSE or MAE indicates a more precise prediction of the model.

L Implementation Details

Device. All our experiments are conducted on a Linux server with 16 NVIDIA A100 Tensor Core GPUs using a multi-thread dataloader and 503G memory.

Hyper-Parameter Settings. We adopt the Bayesian Optimization [24], searching through the parameter hyper-space, and find the lowest nMSE when setting [learning_rate, batch_size, weight_decay, dropout, α , K]=[1e-5, 64, 0.001, 0, 0.8, 10]. We apply the above set of parameters to acquire our result and compare M³TR with other baselines. Hyper-parameter optimization and sensitivity analysis have been discussed in detail in the main paper.

Hyper-Parameters Analysis. After initial adjustments, the model’s performance shows low sensitivity to *weight_decay*, *batch_size* and *dropout*. So we focus on optimizing and analyzing other key parameters: the number of frames captured (K) and the balance between positive and negative attention (α).

Figure 3 illustrates the best nMSE and SRC obtained when training with different values of K and α . The model’s performance is relatively insensitive to these two parameters. M³TR performs best with $K = 10$ and $\alpha = 0.8$. The optimal values for S and lr are 10 and 1e-4, respectively. Overall, our model demonstrates strong robustness.

M More About the Mamba-Hawkes Process

M.1 Case Study: Disentangling the Mamba-Hawkes Process

While quantitative results in the main paper demonstrate the overall superiority of our framework, a deeper qualitative analysis is essential to understand *how* our Mamba-Hawkes Process (MHP) module operates and captures complex temporal dynamics. This case study aims to disentangle the contributions of the classical Hawkes component and the non-linear, Mamba-driven context vector, particularly in a challenging, non-monotonic popularity scenario.

We present a constructed yet representative case of a video that experiences an initial surge in positive engagement, followed by a sudden influx of controversial comments that subsequently suppresses further “Like” activity. Such scenarios, where the valence of user interaction shifts, are notoriously difficult for conventional time-series models. Figure 8 illustrates how our MHP module successfully navigates this complexity.

The visualization reveals the distinct roles of the MHP’s components. The Classic Hawkes Intensity (green, dashed line) correctly

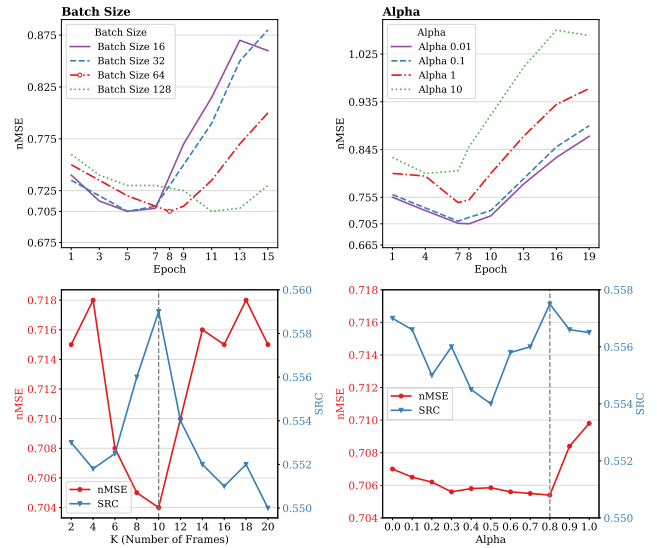


Figure 3: Discussion with different hyper-parameters. The upper two figures show the nMSE during training with different batch sizes and α s. The lower two figure illustrate the nMSE and SRC on testing dataset with different K s and α s.

models the self-exciting nature of Likes (blue markers) and Shares (green markers) during the initial phase ($t=0$ to $t=9$). Each positive event triggers a corresponding spike in the intensity, followed by an exponential decay. However, the fundamental limitation of this classical component is exposed in the second phase ($t>9$). It is oblivious to the semantic shift introduced by the wave of Comments (red markers) and, therefore, fails to predict the subsequent stagnation in user engagement.

This is where Mamba’s Contribution becomes critical. By processing the entire event sequence through its selective state-space mechanism, the Mamba component learns the complex, cross-type event dependencies. Upon observing the influx of comments, it correctly infers a negative context, causing its output, $f_k(h(t))$, to become strongly negative, as shown by the red shaded area. This represents a sophisticated learned dynamic: a burst of controversial comments inhibits future like engagement. The Final MHP Intensity (blue, solid line), which is the synthesis of these two components, is thus corrected. The negative contribution from Mamba effectively counteracts the naive optimism of the classic Hawkes process, pulling the final predicted intensity down to accurately reflect the suppressed user interest.

In summary, this case study validates our core architectural hypothesis. The performance gains of M³TR are not merely a result of using temporal data, but stem from the MHP’s sophisticated ability to model intricate, non-linear interactions between different event types—a capability demonstrably beyond the reach of traditional point process models alone.

M.2 Qualitative Analysis: MHP Dynamics Across Scenarios

To complement our quantitative results and provide a more intuitive understanding of our model’s capabilities, this section presents a qualitative analysis that visually elucidates the superiority of our Mamba-Hawkes Process (MHP) module. We compare the predicted cumulative popularity curves from our M^3TR model against a baseline (a classic Hawkes model) on four distinct and challenging popularity archetypes identified in real-world data.

Figure 4 showcases this comparison. In relatively straightforward scenarios like “Viral Explosion” and “Slow Burn”, both our M^3TR model and the baseline demonstrate competent tracking of the ground truth. Nevertheless, M^3TR ’s predictions maintain a consistently tighter fit, indicating higher precision and robustness.

The critical advantage of our MHP module is starkly revealed in the more complex, non-monotonic scenarios. For the “Flash in

the Pan” case, the baseline model, capable only of modeling self-excitation, incorrectly extrapolates the initial explosive growth, failing to recognize the subsequent stagnation in user engagement. In stark contrast, M^3TR accurately captures this abrupt turning point. This is because the MHP’s Mamba component learns to interpret the influx of later-stage comments (the red “x” markers) as a negative contextual shift, providing a crucial corrective signal to the overall intensity function. Similarly, in the “Sleeper Hit” scenario, M^3TR exhibits superior responsiveness by correctly identifying the delayed take-off point and matching the steep growth trajectory, whereas the baseline model lags.

Collectively, these case studies visually corroborate our quantitative findings. They provide strong evidence that the sophisticated, context-aware architecture of our MHP module is essential for accurately forecasting the full spectrum of complex popularity trajectories, a task where simpler temporal models fundamentally fall short.

MHP Intensity Function vs. Baseline Across Popularity Scenarios

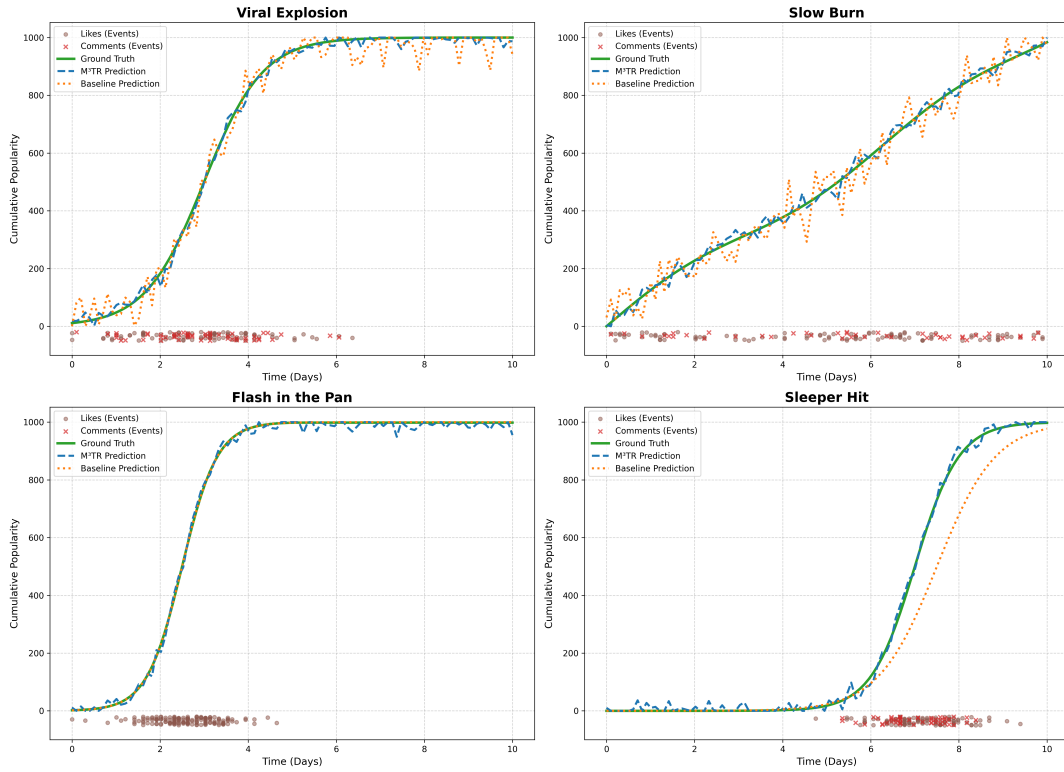


Figure 4: A comparative case study of cumulative popularity prediction across four scenarios. The plots show the Ground Truth (solid green), our M³TR prediction (dashed blue), and a Baseline prediction (dotted orange). Scatter points at the bottom represent the timing of raw user interaction events (Likes and Comments). The “Flash in the Pan” scenario particularly highlights M³TR’s ability to model trend reversals, a key limitation of the baseline.